Sustainable Energy, Grids and Networks 47 (2026) 102418

Contents lists available at ScienceDirect

Sustainable Energy, Grids and Networks

journal homepage: www.elsevier.com/locate/segan

A multi-objective optimization approach to integrated energy network co-planning

Jonathan Vieth [a,*], Johannes Heise [b], Marwan Mostafa [b], Christian Becker [b], Arne Speerforck [a]

[a] Institute of Engineering Thermodynamics, Hamburg University of Technology, Denickestraße 17, Hamburg, 21073, Germany
[b] Institute of Electrical Power and Energy Technology, Hamburg University of Technology, Harburger Schloßstraße 36, Hamburg, 21079, Germany

HIGHLIGHTS

- Extended Energy Hub model for modeling geographic zones.
- Automated extension and parameterization of district heating networks.
- Automated simulation of integrated energy networks.
- Constrained multi-objective optimization of integrated energy networks.

ARTICLE INFO

Keywords:
Energy hub
District heating network modeling
District heating network simulation
Integrated energy network optimization
Co-planning

ABSTRACT

This paper presents a constrained multi-objective optimization approach for the simultaneous extension and operation planning of integrated energy networks. The integrated energy network comprises a district heating network, an electric energy network, a gas network, and decentralized heating technologies such as pellet boilers. The approach dissects the area of interest into zones. Each zone is represented by a novel model based on the *energy hub* concept. Therefore, the approach is scalable and allows for the planning of metropolitan areas. The zones are connected by overlying energy networks. The overlying energy networks and the zones are simulated for one year. The simulation is executed within an optimization. In addition, the approach is capable of accounting for the limits of the integrated energy network's extension. Consequently, it allows for a realistic planning of future integrated energy networks.

1. Introduction

With the *European Green Deal* the European Union has set a target of reducing greenhouse gas emissions by at least 50% by 2030 in comparison to 1990 [1]. In 2021, the building sector in Europe was responsible for 35% of the greenhouse gas emissions [2], requiring a reduction of greenhouse gas emissions in the building sector within a few years.

A variety of technologies are available for supplying buildings with heat. For instance, in the city of Hamburg in 2019, approximately 36.6% of residential buildings were connected to the district heating network (DHN), 30.6% to the gas network, 1.9% of residential buildings were supplied by heat pumps (HPs), and the remaining residential buildings were supplied by heating technologies without a network connection, such as pellet and oil boilersdecentralized heating technologies (e.g., pellet and oil boilers) [3]. Consequently, the decarbonization of the building stock in a metropolitan area has implications for not only the buildings themselves but also the energy networks present.

In the case of DHNs, the producers of the DHNs are primarily responsible for influencing the CO_2 emissions. Large scale HPs (LSHPs) are frequently considered a technology for decarbonizing DHNs (e.g., [4]). However, the efficiency of an LSHP depends on the source and sink temperature [5], i.e., on the supply temperature of the DHN. Therefore, the extension and producer planning of a DHN necessitate the consideration of the operation of the DHN. Heendeniya et al. [6] introduced the term *co-planning*, which describes the simultaneous consideration of extension and operational planning of integrated energy networks (IENs).

* corresponding author.
Email addresses: jonathan.vieth@tuhh.de (J. Vieth), johannes.heise@tuhh.de (J. Heise), marwan.mostafa@tuhh.de (M. Mostafa), c.becker@tuhh.de (C. Becker), arne.speerforck@tuhh.de (A. Speerforck).

https://doi.org/10.1016/j.segan.2026.102418
Received 22 January 2026; Received in revised form 15 June 2026; Accepted 10 July 2026
Available online 14 July 2026

Nomenclature

Variables

n, m	number of
$\mathcal{Z}$	set of geographic zones
$\mathcal{Y}$	set of new producers
$\mathcal{G}$	graph
$\mathcal{N}$	set of nodes
$\mathcal{E}$	set of edges
$\mathcal{H}$	set of houses
$\mathcal{D}$	set of possible pipe diameters
$\mathcal{P}$	set of possible heating system sizes
$\mathcal{C}$	set of CAPEXs
$\mathcal{L}$	set of power lines
$\mathcal{O}$	set of CO_2 prices
$o(e)$	origin of edge e
$t(e)$	tail of edge e
$x(n)$	horizontal geo-coordinate of node n
$y(n)$	vertical geo-coordinate of node n
$l(e)$	geographic length of edge e
$\boldsymbol{x}$	vector of optimization variables
y	expansion planning variables
u	operation planning variables
P	power
E	energy
k	time step
T	temperature
Δ	difference
η	efficiency factor
d	diameter
ϵ	pipe roughness
U	thermal transmittance
λ	pipe friction factor
ρ	density of water
$\dot{m}$	mass flow
$\dot{Q}$	heating power
Q	heat energy
v	velocity
p	pressure
ζ	loss coefficient
γ	electric power share
η	constant efficiency factor
Θ	homomorphism for linking supply with return nodes
β, ξ	electric power loss multiplication factors
$\hat{\xi}$	constant electric power loss multiplication factor
ψ	constant coefficient of HP part load degradation
c_w	heat capacity of water
t	time
c	CAPEX
$\hat{c}$	specific cost
a	annualized CAPEX
σ	parameters for calculating the annualized CAPEX
ω	lifetime
i	electric current
J	objective function
r	maximum added power line/pipe length per year
s	maximum number of added heating systems per year
A	area

Subscripts

EH	energy hub
PR	producer
ho	house
sq	status quo
opt	DHN graph determined in optimization loop
top	topological model of DHN
sim	simulation model of DHN
r	return line of DHN
$\mathcal{N}$	nodes
$\mathcal{E}$	edges
DHN	district heating network
HP	heat pump
O	decentral heating technologies
GAS	gas
el	electric
h	heat
source	source of heat pump
supply	supply of heat pump
PL	part load of heat pump
C0	Carnot
air	air
soil	soil
pu	pump
all	all possible connections
st	Steiner tree
p	pipe
HS	house station
HV	high voltage
MV	medium voltage
LV	low voltage
BR	branch
CHP	gas fired combined heat and power plants
LSHP	large scale heat pumps
W	waste
o	origin of edge
t	tail of edge
max	maximum
min	minimum
des	desired
tot	total
ts	time step
inv	investment
op	operation
fuel	fuel
PC	power line
TF	transformer
pn	electric energy network
new	new
py	planning years
CO_2	CO_2
cost	annualized CAPEX
Σ	sum of heating technologies

Abbreviations

IEN	integrated energy network
DHN	district heating network
HP	heat pump
EH	energy hub
HV	high voltage
MV	medium voltage
LV	low voltage
HS	house station
COP	coefficient of performance of heat pump
CHP	gas fired combined heat and power plants
LSHP	large scale heat pumps
GB	gas boiler
PB	pellet boiler
MINLP	mixed-integer nonlinear program
CAPEX	capital expenditures

1.1. Challenges of optimal IEN co-planning

In the following, several challenges are discussed that arise when planning the IEN of a metropolitan area, with a focus on IENs that include a DHN.

Challenge 1: Number of states and optimization variables. The majority of optimal DHN planning methods focus on small districts. For example, Morvaj et al. [7] presented an approach for the co-planning problem using a linear optimization approach. The use case consists of twelve houses, resulting in an optimization problem with more than 80 000 states. In [8], a multi-objective optimization approach for the co-planning problem was used in order to consider both economic and environmental objectives. The use case is a small district with only 169 buildings. Vieth et al. [9] presented a toolchain for DHN co-planning based on GIS data. First, an optimal DHN topology is generated from the GIS data. Next, the DHN is simulated in an optimization loop using the simulation model presented in [10], with alterations to the operation and diameters of the supply and return pipes. The result is an optimally parameterized DHN with a matching optimal supply temperature. However, a preexisting DHN is not considered. Additionally, the work solely focuses on DHNs, and a comparison with other heating technologies is not included. Hering et al. [11] introduced a mixed-integer quadratically constrained optimization problem for the design optimization of a DHN. In order to solve the challenging optimization problem, the spatial resolution of the DHN is omitted. However, the main DHN of a metropolitan area usually has several power plants distributed throughout the network. For instance, Grenoble's DHN has three power plants that supply over 1000 consumers [12]. An even larger DHN is that of Turin, which has four thermal plants that supply 5500 buildings and has a total piping length of approximately 2500 km [13]. Therefore, due to the spatial extent of DHNs in metropolitan areas and the number of generation units, it is infeasible to omit the spatial resolution or model each pipe and consumer individually.

In [14,15], metropolitan areas are divided into geographic zones. Di Shi and Tylavsky [14] developed an aggregation method for electric energy networks. In this method, the topology is simplified by merging all nodes in the same zone into one node. Additionally, they present a clustering methodology for selecting zones. While this methodology appears promising, it only applies to electric energy networks. To incorporate the energy networks of the metropolitan area, [15] connects the zones by an overlying IEN and models each zone by an energy hub (EH). An EH is a simplified modeling concept for IENs, as introduced in [16]. The EH approach describes the transformation, storage, and consumption of energy in one centralized unit, the EH. The approach presented in [15] has two limitations. Firstly, no DHN is considered. The addition of a DHN to the concept presented in [15] is challenging due to the absence of network levels in DHNs, in contrast to electric energy and gas networks. For example, electric energy networks can span several countries. Electricity is transported over long distances through transmission lines at high voltages. Residential consumers, however, are usually connected to low-voltage grids. Transformers connect the different network levels (voltage levels in electric energy networks and pressure levels in gas networks).

Secondly, the concept presented in [15] is a black-box model from a network point of view. No information is available regarding the electric energy network, gas network, and DHN within each EH. It is only possible to estimate power losses and overloads from power demands.

In [17], the case study is the DHN in Turin, Italy, one of the largest DHNs in Europe. The goal is to study whether it is feasible to extend the existing DHN. However, only hydraulic restrictions are considered. Furthermore, the extension is only tested and not run in an optimization loop.

Challenge 2: Nonlinear system dynamics. In the case of DHNs, the governing equations are nonlinear. Therefore, assumptions have to be made in order to achieve a linear optimization problem for the planning of IENs containing a DHN. Cao et al. [18] assumed a constant mass flow within the DHN in order to achieve a linear optimization problem. However, apart from the supply temperature, the mass flow is the most important control variable in DHNs, since the power consumption of DHN house stations is usually controlled by a control valve and thus by manipulating the mass flow through the house station [19]. Hence, the assumption of a constant mass flow is not practical. Hauk et al. [20] presents a co-planning approach for IENs considering preexisting networks. By neglecting network losses, the procedure results in a linear optimization problem. However, minimizing network losses is one of the main tasks in planning IENs, as pointed out in [21]. Hence, omitting network losses is not feasible.

In conclusion, a nonlinear model is required to adequately represent an IEN containing a DHN.

Challenge 3: Considering the status quo and extension limits. As previously stated, the greenhouse gas emissions of the building sector must be reduced significantly within a relatively short period of time. Consequently, in metropolitan areas, the planning of the future energy networks must be based on the preexisting networks, given that network extension is a time-consuming process. Furthermore, a co-planning approach is required considering the limits of the network extension, as well as the limits of the addition of boilers, DHN house stations (HSs), and HPs. In [17], the extension of an existing DHN is tested considering only hydraulic restrictions. The test case in [20] consists of 900 buildings, requiring the consideration of the low voltage (LV)LV and the MV level of the electric network. The interconnection of the energy networks through coupling technologies such as LSHPs occurs in the electric network at medium voltage (MV)MV and high voltage (HV)HV voltage levels. The neglect of the LV voltage level is not possible, due to the interaction of the voltage levels, as pointed out by [20]. However, the amount of LV lines is usually huge compared to MV and HV lines. Considering the LV level massively increases the complexity of the problem. Hauk et al. [20] solved the problem by introducing an aggregation algorithm. Each group of buildings is aggregated to one building. The line length is calculated as a weighted average of all line distances from each building to the transformer, with the annual energy demand as the weighting factor. In [7,11], the goal is to find the optimal network for a set of houses. An extension of existing networks as in [17,20] is not considered.

In summary, most of the existing methods for planning IENs do not take into account the existing networks, as the focus is on decarbonizing the heat demand of a small district [7,8,11]. Other methods use simplifications such as neglecting the losses [20] or omitting the spatial resolution [11], which is not feasible when developing a method for the planning of IENs for a metropolitan area. Therefore, there is a lack of methods that address the extension planning of IENs in metropolitan areas using physical network models.

1.2. Optimization approaches

In general, there are two approaches to co-planning of IENs [22]. The approaches presented in [7,11,20] formulate the co-planning problem as a mixed-integer optimization problem, where the physics behind the networks are contained in the constraints of the optimization problem. A second approach is used in [8,23,24], where the IENs are simulated for a representative time interval and the results of the simulation are processed by an optimization algorithm, such as a genetic or a surrogate algorithm.a genetic algorithm. These optimization algorithms then identify new points for evaluation based on previously evaluated points. For an introduction to surrogate optimization algorithms, see [25], and for an introduction to genetic algorithms, see [26].

The second approach has several advantages. First, as pointed out in [8], only a simulation can handle the complex restrictions typically present in IENs without significantly increasing the mathematical complexity. Second, in the case of extension planning of IENs, a typical problem is to find the shortest pipe or power line extension connecting consumers with producers. From a mathematical point of view, the solution to this problem is a *Steiner tree*. Finding the Steiner tree is an NP-complete problem [27]. If an optimization approach is used, where the networks of the IEN are part of the constraints, finding the optimal pipe or power line extension has to be added to the already complex optimization problem. In the case of a simulation, a Steiner tree approximation algorithm, as presented in [27], can be run prior to the simulation. The disadvantage of a simulation-based optimization is the robustness of the approach. Especially in the case of DHNs with more than one generation unit, the mass flows in each generation unit and the supply temperatures at each generation unit must be well chosen to obtain realistic results. This becomes even more challenging when the DHN topology changes due to the extension planning of the IEN.

As discussed in *Challenge 2*, nonlinear models are necessary for adequately representing IENs. One option when using mixed-integer optimization is to relax these nonlinear constraints. Adjoint methods for optimally designing DHNs and gas networks, respectively, were presented in [28,29]. These methods optimize mass flow configurations by altering geometries, such as pipe diameters [29]. Based on [28,30] it was demonstrated that using a *pipe penalization approach* reduced the time required to find the optimal DHN from 46 min to 11 min. A different novel approach was presented in [31]. In this work, a primal decomposition technique was used to accelerate the optimization of thermo-hydraulic systems. Similar to [18], assuming constant mass flows achieves a linear optimization problem. Iteratively altering the mass flows achieves a more scalable approach than directly solving the nonlinear optimization problem.

Although promising methods for relaxing the nonlinear constraints were presented in [32] and in [31] for example for DHNs, the advantages of the optimization approaches using simulations in combination with genetic or surrogate algorithms still prevail.

1.3. Contribution

This paper presents a *constrained multi-objective optimization approach* for the co-planning of the IEN of a metropolitan area. All three energy networks (district heating, gas, and electric energy network) are modeled and simulated. Therefore, the spatial resolution of the metropolitan area is incorporated. A genetic and a surrogate algorithm are then used to process the results of the simulations and find the optimal IEN configuration. The optimization problem is constrained by the extension limits of the networks and of the heating technologies. The approach uses the existing IEN as a starting point.

Since it is not feasible to simulate an IEN in which every house in the metropolitan area is modeled, an aggregation of houses into zones is developed, similar to [15,20]. In contrast to [20], zones is developedses into zones incorporates network losses. By modifying the number of zones, the computation time and the accuracy of the optimization are affected. Therefore, the approach presented in this work is scalable with respect to the number of consumers in the metropolitan area.

The contribution of this work is as follows

- An aggregation method for IENs to zones based on EHs.
- The automated extension and one year simulation of IENs with multiple generation units including waste incineration plants, gas powered combined heat and power (CHP) plants, and LSHPs.
- A constrained multi-objective optimization method for IENs considering pre-existing networks.

1.4. General procedure

The general procedure is depicted in Fig. 1. The input of the parameterization and simulation is the vector $\boldsymbol{u}$ of the operation planning variables and the vector $\boldsymbol{y} = \begin{bmatrix}\boldsymbol{y}_{\mathrm{EH}}^{\top} & \boldsymbol{y}_{\mathrm{PR}}^{\top}\end{bmatrix}^{\top}$ of the extension planning variables. The variables contained in $\boldsymbol{u}$ influence the operation of the coupling technologies (e.g., LSHPs and CHPs) via a *rule-based control* as described in Section 3.4. The extension variables $\boldsymbol{y}_{\mathrm{EH}}$ influence the allocation of houses to the four heating technologies: HPs, DHN HSs, gas boilers, and pellet boilers. The assignment of houses to heating technologies influences the dimensioning and topology of the three networks: DHN, electric network, and gas network. The extension variables $\boldsymbol{y}_{\mathrm{PR}}$ affect the addition of coupling technologies. All three networks are simulated for one year. The output of the simulation is the imported gas and electric power for each time step, the required extension and reinforcement of the IEN, and the added heating technologies. Based on the simulation results, the CO_2 emissions and the total annualized cost of the IEN extension can be calculated.

1.5. Notation

Given is a set $\mathcal{A} = \{1, 2, 3\}$. The operator $\begin{bmatrix}a_i\end{bmatrix}$ for all i in $\mathcal{A}$ denotes the vector

$$\boldsymbol{a} = \begin{bmatrix}a_1 & a_2 & a_3\end{bmatrix} = \begin{bmatrix}a_i\end{bmatrix}, \quad \forall i \in \mathcal{A}.$$

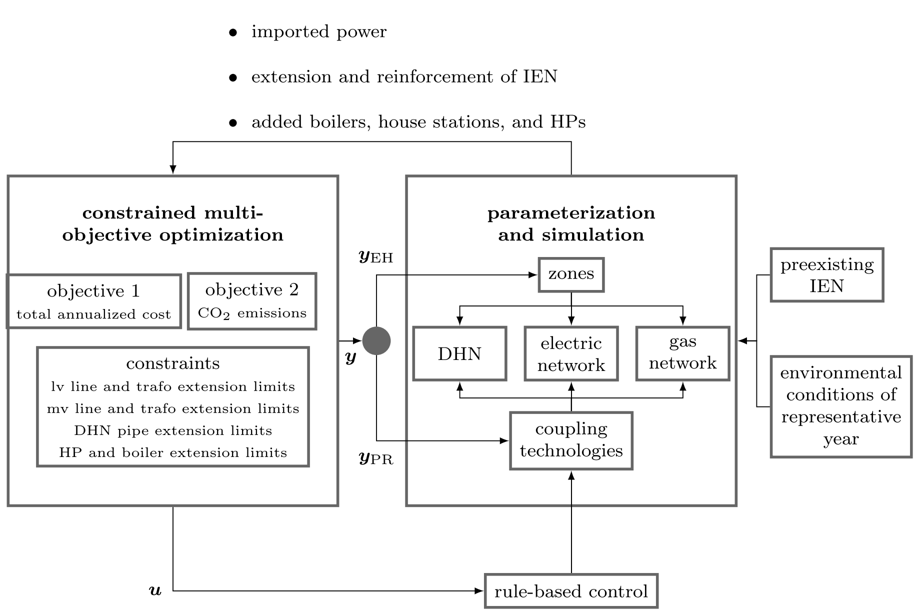

Fig. 1. General procedure of the co-planning approach.

2. Network model

In this work, we present a novel and scalable approach to the modeling of the IEN of a metropolitan area. To achieve scalability, the metropolitan area is divided into $n_{\mathrm{EH}} = |\mathcal{Z}|$ geographic zones given by the set $\mathcal{Z}$. Similar to [15], the geographic zones are interconnected by an overlying IEN consisting of an electric energy network, a gas network, and a DHN. The gas and electric energy networks are connected to the higher network level, allowing for the import of additional power from outside the metropolitan area. Each zone is modeled by a novel extended EH presented in Section 2.2. Subsequently, the methodology for modeling the overlying IEN connecting the geographic zones is presented in Section 2.3. In Section 2.1, assumptions regarding the heating technologies and the status quo of the IEN are discussed.

2.1. Assumptions

Several assumptions have been made. It is assumed that the available heating technology options are gas boilers, HPs, a connection to the DHN, and pellet boilersdecentralized heating technologies. Note that other heating technologies that do not require a network connection can also be added without altering the general procedure. The result of the IEN co-planning depends on the status quo of the IEN. It is assumed that all zones are already connected to the electric energy and gas networks. Consequently, the topology of the gas and electric energy networks remains unchanged. Nevertheless, reinforcement of existing electric energy network connections is possible. The modeling of the electric energy network is based on the assumption that both the MV and the LV networks are operated exclusively in a radial manner , which is valid for conventional power networks [33]. It is also assumed that each feeder is of equal length and has the same number of consumers. This assumption is generally not valid, but it is justified in order to achieve a scalable optimization model. This assumption needs to be relaxed in future work. In the case of the electric energy network, this assumption is not a limitation, as the vast majority of buildings in metropolitan areas are connected to the electric energy network. The availability of a gas network depends on the location of the metropolitan area. For example, in Germany, gas is the most common heating option. Hence, the assumption is valid. If gas networks are not a common heating technology, the methods used in this work for DHNs are also valid for gas networks.

2.2. Modeling the geographic zones

This section introduces the novel EH model, as shown in Fig. 2. The novel EH concept models the LV and MV electric energy networks using simplified topologies, comparable to the approach in [20]. However, in contrast to [15,16,20], physically realistic line, transformer, HS, and pipe models are used in order to incorporate realistic losses and overloads. Since there are no gas power losses in gas networks, a power balance for the gas network within each geographic zone is sufficient.

Due to the physical models, the presented novel EH is computationally more expensive than the traditional EH model presented in [16]. However, by appropriately choosing the size of each zone, the presented method is scalable.

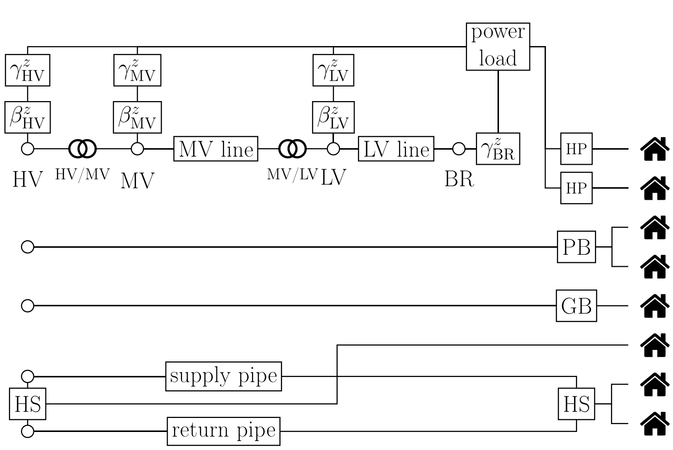

Fig. 2. Representation of EH z. The conventional electrical load of the houses is not depicted.

2.2.1. Electric energy network within the zones

All electric house demands in the EH are aggregated into one load. HPs are modeled separately in order to consider part load behavior (see Section B.2). Hence, in contrast to [15,16], all houses each have a distinct heating demand profile.

Unlike the EH models presented in [15,16], this model explicitly considers overloads and losses by incorporating physical models of one branch of an LV-network and one branch of an MV-network. Each branch is represented by a power line and a transformer (Fig. 2). The electric demand is distributed among four buses of the electric energy network within the EH. The electric power load $P^z_b = \gamma^z_b P^z_{\mathrm{el}}$ is allocated to the bus $b \in \{\mathrm{HV}, \mathrm{MV}, \mathrm{LV}, \mathrm{BR}\}$ of the electric energy network within the EH (Fig. 2), where P^z_{el} is the electric power load of EH z. The electric power share γ^z_b is given by the share of houses connected solely to bus b, i.e., $\gamma^z_b = \frac{n^z_b}{n^z_{\mathrm{ho}}}$ with n^z_b the number of houses connected to bus b. Following, a formula for calculating γ^z_b for each $b \in \{\mathrm{HV}, \mathrm{MV}, \mathrm{LV}, \mathrm{BR}\}$ is derived.

It is assumed that each LV-network consists of m_{BR} branches and each MV-network consists of m_{LV} LV-networks. In EH z, each branch supplies n^z_{BR} houses. Therefore, $\gamma^z_{\mathrm{BR}} = \frac{n^z_{\mathrm{BR}}}{n^z_{\mathrm{ho}}}$ and

$$\gamma^z_{\mathrm{LV}} = \frac{(m_{\mathrm{BR}} - 1) n^z_{\mathrm{BR}}}{n^z_{\mathrm{ho}}}.$$

If EH z contains exactly one HV-network, i.e., $m^z_{\mathrm{HV}} = 1$, γ^z_{MV} represents the load of $n^z_{\mathrm{ho}} - m_{\mathrm{BR}} n^z_{\mathrm{BR}}$, i.e.,

$$\gamma^z_{\mathrm{MV}} = \frac{n^z_{\mathrm{ho}} - m_{\mathrm{BR}} n^z_{\mathrm{BR}}}{n^z_{\mathrm{ho}}}$$

and $\gamma^z_{\mathrm{HV}} = 0$. If $m^z_{\mathrm{HV}} > 1$, it is assumed that each MV-network in EH z supplies $n^z_{\mathrm{MV}} = \frac{n^z_{\mathrm{ho}}}{m^z_{\mathrm{MV}}}$ houses. Each LV-network contains $m_{\mathrm{BR}} n^z_{\mathrm{BR}}$ houses. Hence, $(m_{\mathrm{LV}} - 1) m_{\mathrm{BR}} n^z_{\mathrm{BR}}$ houses are solely connected to bus MV and therefore

$$\gamma^z_{\mathrm{MV}} = \frac{(m_{\mathrm{LV}} - 1) m_{\mathrm{BR}} n^z_{\mathrm{BR}}}{n^z_{\mathrm{ho}}}.$$

All remaining $n^z_{\mathrm{ho}} - n^z_{\mathrm{MV}}$ houses are considered by

$$\gamma^z_{\mathrm{HV}} = \frac{n^z_{\mathrm{ho}} - n^z_{\mathrm{MV}}}{n^z_{\mathrm{ho}}}.$$

Since not all loads are connected to bus BR, additional power losses have to be added to all loads except the ones considered by γ_{BR}. Hence, the loads connected to HV, MV, and LV, are multiplied by

$$\beta^z_b \left(P^z_{\mathrm{el}}(k)\right) = 1 + \xi^z_b \left(P^z_{\mathrm{el}}(k)\right) P^{z\,2}_{\mathrm{el}}(k), \forall b \in \{\mathrm{HV}, \mathrm{MV}, \mathrm{LV}\}$$

with

$$\xi^z_b \left(P^z_{\mathrm{el}}(k)\right) = \hat{\xi}_b \frac{\sum_k P^z_{\mathrm{el}}(k)}{\sum_k P^{z\,2}_{\mathrm{el}}(k)},$$

where $\hat{\xi}_b$ is the loss factor corresponding to the load at bus b. The loss factors were estimated using the model from this paper by the same authors [34]. For all simulations the loss factors are set to $\hat{\xi}_{\mathrm{LV}} = 0.04\ \mathrm{W}^{-1}$, $\hat{\xi}_{\mathrm{MV}} = 0.05\ \mathrm{W}^{-1}$, and $\hat{\xi}_{\mathrm{HV}} = 0.055\ \mathrm{W}^{-1}$.

2.2.2. District heating network within the zones

The DHN in each EH consists of a supply pipe, a return pipe, and two HSs, as depicted in Fig. 2. The y^z_{DHN} end-users connected to the DHN in EH z are represented by the two HSs. Assuming a consistent geographic distribution of the houses within each EH, the demand of the y^z_{DHN} houses is split equally between both HSs.

The topology consisting of a supply pipe, a return pipe, and two HSs can be understood as a universal topology for DHNs, since it is the topology with the fewest possible elements resulting from the aggregation algorithm presented in [35]. Therefore, it is used for modeling the geographic zones. The parameters of the model are the diameter, the length and the friction factor of each pipe, resulting from the aggregation algorithm developed in [35].

2.2.3. Gas network and pellet boilersdecentralized heating options within the zones

Since power losses do not occur during gas networks in regular operation and we assume no overload of the gas pipes, a power balance for the gas network representation within the EHs is sufficient. For the pellet boilersdecentralized heating options a power balance is considered as well.

2.3. Modeling the interconnecting networks

After deriving a simplified modeling approach for the geographic zones, the modeling of the IEN connecting the geographic zones is described. The overlying IEN is modeled using state of the art modeling tools for all three energy networks, ensuring that the spatial distribution and the efficiencies of the IEN are represented. A common approach for modeling energy networks is graphs [36–39]. The notation concerning graphs is based on [40]. Whenever *graphs* are mentioned, the graph has no parallel edges and no loops. A graph is defined as a tuple $\mathcal{G} = (\mathcal{N}, \mathcal{E})$ with the set of nodes $\mathcal{N}$ and set of edges $\mathcal{E}$. The origin of each edge $e \in \mathcal{E}$ is denoted by $o(e) \in \mathcal{N}$ and the tail by $t(e) \in \mathcal{N}$. In addition to [40], each node $n \in \mathcal{N}$ has a specific horizontal $x(n)$ and vertical $y(n)$ geographic coordinate. The geographic distance between two nodes $a, b \in \mathcal{N}$ is given by

$$l(\overline{ab}) = l(e) = \sqrt{(x(a) - x(b))^2 + ((y(a) - y(b))^2},$$

with $e = (a, b) \in \mathcal{E}$.

2.3.1. Electric energy and gas networks

For electric energy and gas networks we assume that nodes correspond to the zones, producers, connections to external networks, or simple connection points, which is a common approach when using a quasi-stationary modeling approach [41–43]. The electric energy and gas networks are modeled by the two connected, directed graphs $\mathcal{G}_{\mathrm{el}} = (\mathcal{N}_{\mathrm{el}}, \mathcal{E}_{\mathrm{el}})$ and $\mathcal{G}_{\mathrm{GAS}} = (\mathcal{N}_{\mathrm{GAS}}, \mathcal{E}_{\mathrm{GAS}})$, respectively.

2.3.2. District heating network

For the DHN, two models are considered: A *simulation model* $\mathcal{G}_{\mathrm{sim}}$, where edges correspond to pipes, geographic zones, and producers. Nodes are simple connection points of the edges. A *topological model* $\mathcal{G}_{\mathrm{top}}$ where nodes correspond to producers and geographic zones and edges correspond to DHN lines. Hence, in $\mathcal{G}_{\mathrm{top}}$ each edge represents a supply pipe as well as a return pipe of the DHN. A more formal definition of $\mathcal{G}_{\mathrm{sim}}$ and $\mathcal{G}_{\mathrm{top}}$ is given in Appendix A.

3. Simulation model

This section provides a detailed description of the simulation model called in each iteration of the optimizer. Calling a simulation in each iteration of the optimizer instead of formulating the problem as a *mixed-integer nonlinear problem* is justified in Section 1.2. The core of the simulation model is the simulation of a representative year of the IEN modeled by the novel EH model and the overlying IEN, as depicted in

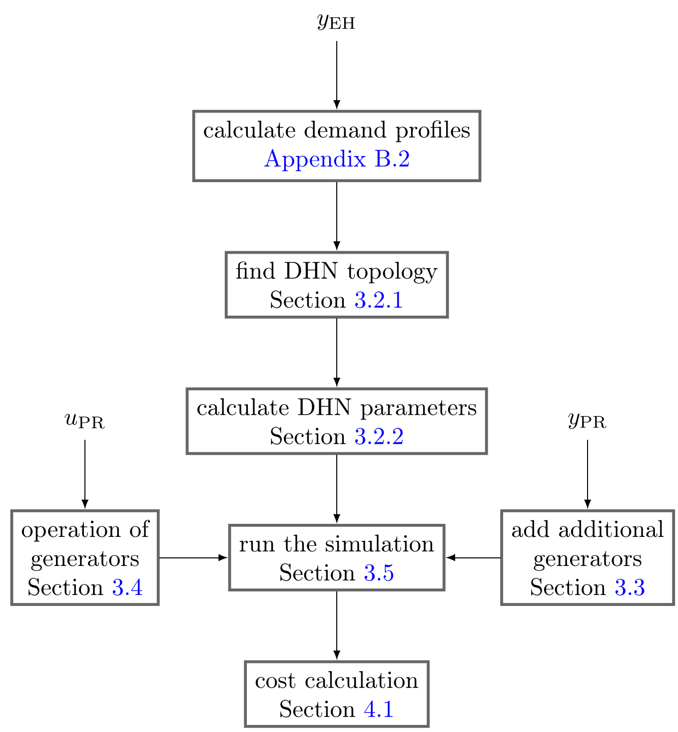

Fig. 3. Procedure of the parameterization and simulation.

Fig. 1. All simulations are performed in *pandapower* [39] and *pandapipes* [44]. Prior to simulating, the IEN must be parameterized based on the design variables. The sequence of steps involved in running the simulation model is depicted in Fig. 3. Based on the design variables the simulation model calculates

- electric energy network overloads
- extension of the DHN
- imported electric energy, gas, and energy for pelletsdecentralized heating technologies
- temperatures at all junctions of the DHN
- yearly operating cost of the IEN

As illustrated in Fig. 1, the outputs of the simulation model are used for calculating the objectives (total annualized cost and CO_2 emissions) and the constraints (limits of the IEN extension).

3.1. Design variables

The design variables $\boldsymbol{x}$ of a co-planning process for IENs contain design variables u of the operation and design variables y of the extension [6]. The vector of design variables $\boldsymbol{x} = \left[\boldsymbol{y}^{\top}_{\mathrm{EH}} \quad \boldsymbol{y}^{\top}_{\mathrm{PR}} \quad \boldsymbol{u}^{\top}_{\mathrm{PR}}\right]^{\top}$ contains first the vector $\boldsymbol{y}_{\mathrm{EH}} = \left[\boldsymbol{y}^{\top}_{\mathrm{HP}} \quad \boldsymbol{y}^{\top}_{\mathrm{DHN}} \quad \boldsymbol{y}^{\top}_{\mathrm{GAS}}\right]^{\top}$ describing the number of houses connected in each zone to the three technologies: electric energy network via HP (HP), district heating (DHN), and gas network via gas boilers (GAS). For each $t \in \{\mathrm{HP}, \mathrm{DHN}, \mathrm{GAS}\}$ the vector $\boldsymbol{y}_t = \left[y^z_t\right]$ for all $z \in \mathcal{Z}$ is given, where y^z_t is the number of houses in zone z connected to technology t. The remaining houses

$$\boldsymbol{y}_{\mathrm{O}} = \boldsymbol{n}_{\mathrm{ho}} - \sum_{t \in \{\mathrm{HP}, \mathrm{DHN}, \mathrm{GAS}\}} \boldsymbol{y}_t \tag{1}$$

with $\boldsymbol{n}_{\mathrm{ho}} = \left[n^z_{\mathrm{ho}}\right]$ for all $z \in \mathcal{Z}$ are supplied by pellet boilersdecentralized heating options, where n^z_{ho} denotes the number of houses in EH z.

The second input vector $\boldsymbol{y}_{\mathrm{PR}} = \left[y^g_{\mathrm{PR}}\right]$ for all $g \in \mathcal{Y}_{\mathrm{opt}}$ describes the maximum heating power, where $\mathcal{Y}_{\mathrm{opt}}$ is the set of producers that may be added by the optimizer.

Third, the vector $\boldsymbol{u}_{\mathrm{PR}}$ contains operational parameters for the producers described in more detail in Section 3.4.

3.2. Parametrization of the DHN

In case an EH is newly connected to the DHN, the parameters of the newly added pipes have to be calculated. For running a simulation, pandapipes requires for each pipe p length l_p, diameter d_p, pipe roughness ϵ_p, and a thermal transmittance U_p. The pipe material coefficient ϵ_p is assumed to be constant over all pipes with $\epsilon_p = \epsilon = 0.2$ mm. The parameter U_p is set to $U_p = \frac{0.15 \text{ W m}^{-1} \text{ K}^{-1}}{\pi d_p}$. In the upcoming two paragraphs, we first present a procedure for calculating l_p of each added pipe p and afterwards for calculating d_p.

3.2.1. Finding the DHN topology

When connecting an EH z to the graph $\mathcal{G}_{\mathrm{top}}^{\mathrm{sq}}$, which describes the topology of the status quo DHN, the optimal connection point on $\mathcal{G}_{\mathrm{top}}^{\mathrm{sq}}$ must to be found. Hence, the goal is determine the optimal DHN topology $\mathcal{G}_{\mathrm{top}}^{\mathrm{opt}} = \left(\mathcal{N}_{\mathrm{top}}^{\mathrm{opt}}, \mathcal{E}_{\mathrm{top}}^{\mathrm{opt}}\right)$ interconnecting all EHs with DHN loads, i.e.,

$$\mathcal{N}_{\mathrm{top,EH}}^{\mathrm{opt}} = \left\{ z \in \mathcal{N}_{\mathrm{all}}^{\mathrm{EH}} \mid y_{\mathrm{DHN}}^{z} > 0 \right\}.$$

The decision is made based on an objective function. In this work the objective of the optimization is solely based on the added piping length. Consequently, the optimization problem

$$\min_{\mathcal{G}_{\mathrm{top}}^{\mathrm{opt}}} \sum_{e \in \left(\mathcal{E}_{\mathrm{top}}^{\mathrm{opt}} \setminus \mathcal{E}_{\mathrm{top}}^{\mathrm{sq}}\right)} l(e) \tag{2a}$$

$$\text{s.t.} \quad \mathcal{N}_{\mathrm{top,EH}}^{\mathrm{opt}} \subset \mathcal{N}_{\mathrm{top}}^{\mathrm{opt}} \tag{2b}$$

$$\mathcal{G}_{\mathrm{top}}^{\mathrm{opt}} \text{ is connected} \tag{2c}$$

$$\mathcal{G}_{\mathrm{top}}^{\mathrm{opt}} \subset \left(\mathcal{G}_{\mathrm{top}}^{\mathrm{sq}} \cup \mathcal{G}_{\mathrm{top}}^{\mathrm{all}}\right) \tag{2d}$$

$$\mathcal{G}_{\mathrm{top}}^{\mathrm{sq}} \subset \mathcal{G}_{\mathrm{top}}^{\mathrm{opt}} \tag{2e}$$

must be solved in order to find the DHN topology. The length of an edge e is given by $l(e)$ which is calculated by the distance between $o(e)$ and $t(e)$. The search for the optimal $\mathcal{G}_{\mathrm{top}}^{\mathrm{opt}}$ is based on the graph $\mathcal{G}_{\mathrm{top}}^{\mathrm{all}}$ which contains all possible routes for DHN connections. This might represent the street network of the metropolitan area and is assumed to be known. Eq. (2a) is the objective, (2b) ensures that all zones with DHN loads are connected to the DHN, (2c) describes the requirement that all zones are supplied by one DHN, (2d) states that only edges contained in $\mathcal{G}_{\mathrm{top}}^{\mathrm{all}}$ can be added to the DHN, and (2e) ensures that all edges of the status quo DHN are included in the optimal DHN topology.

Two steps are required for finding $\mathcal{G}_{\mathrm{top}}^{\mathrm{opt}}$. Firstly, the optimization problem (2a)–(2d) is solved. The graph $\mathcal{G}_{\mathrm{top}}^{\mathrm{st}}$ is the *minimum Steiner tree* of graph $\mathcal{G}_{\mathrm{top}}^{\mathrm{sq}} \cup \mathcal{G}_{\mathrm{top}}^{\mathrm{all}}$ with the set of terminal nodes $\mathcal{N}_{\mathrm{top,EH}}^{\mathrm{opt}}$. Therefore, $\mathcal{G}_{\mathrm{top}}^{\mathrm{st}}$ is the solution to the optimization problem (2a)–(2d). For finding $\mathcal{G}_{\mathrm{top}}^{\mathrm{st}}$ the Steiner tree approximation algorithm presented in [27] implemented in the Python package *NetworkX* is used [45].

Then, the DHN topology is given by

$$\mathcal{G}_{\mathrm{top}}^{\mathrm{opt}} = \mathcal{G}_{\mathrm{top}}^{\mathrm{st}} \cup \mathcal{G}_{\mathrm{top}}^{\mathrm{sq}}, \tag{3}$$

which satisfies constraint (2e). Joining the two graphs in (3) is necessary, since possible loops in $\mathcal{G}_{\mathrm{top}}^{\mathrm{sq}}$ will not occur in $\mathcal{G}_{\mathrm{top}}^{\mathrm{st}}$. An example of $\mathcal{G}_{\mathrm{top}}^{\mathrm{all}}$, $\mathcal{G}_{\mathrm{top}}^{\mathrm{sq}}$, and $\mathcal{G}_{\mathrm{top}}^{\mathrm{opt}}$ is shown in Fig. 4(a).

3.2.2. Calculating the DHN parameters

After finding the topology $\mathcal{G}_{\mathrm{top}}^{\mathrm{opt}}$ in Section 3.2.1, next the parameters of the DHN have to be calculated. Hence, the goal is to find the simulation model $\mathcal{G}_{\mathrm{sim}}^{\mathrm{opt}}$ from $\mathcal{G}_{\mathrm{top}}^{\mathrm{opt}}$.

Pipe lengths. The length of each edge $e \in \left(\mathcal{E}_{\mathrm{top}}^{\mathrm{opt}} \cup \mathcal{E}_{\mathrm{r}}^{\mathrm{opt}}\right)$ is known due to the distances between the nodes. As described in Section 2.2, each EH consists internally of two pipes and two HSs. Each HS again is modeled by a valve, a pump, and a heat exchanger. Since the length $l(e)$ of $e \in \mathcal{E}_{\mathrm{EH}}$ is the result of an aggregation, $l(e)$ depends on y_{DHN}^{h}, where h is the EH represented by e (see Fig. 2 for the structure of the DHN within the EHs). Since we do not want to run an aggregation in each optimization loop, all needed aggregations can be performed in advance. Hence, a mapping $y_{\mathrm{DHN}}^{h} \to l(h)$ is assumed to be known for each EH h.

The unaggregated piping length $l_{\mathrm{p,EH}}^{h}$ of the DHN in each EH is still needed to calculate the investment cost. The procedure for calculating pipe investment costs is explained in Appendix C.1.2, and the case study parameters for each EH are given in Table 1.

Diameters. In each optimization loop, the diameter vector of added pipes

$$\boldsymbol{d}_{\mathrm{opt}} = \begin{bmatrix} d_{\mathrm{opt}}^{1} & d_{\mathrm{opt}}^{2} & \dots & d_{\mathrm{opt}}^{n_{\mathrm{opt,p}}} \end{bmatrix}$$

with $n_{\mathrm{opt,p}} = \left|\mathcal{E}_{\mathrm{top}}^{\mathrm{opt}} \setminus \mathcal{E}_{\mathrm{top}}^{\mathrm{sq}}\right|$ has to be chosen out of the set $\mathcal{D}$ of possible diameters. This task can be formulated as a *mixed-integer nonlinear program* (MINLP). However, solving a MINLP is time consuming. Hence, the calculation takes place based on a desired velocity $v_{\mathrm{des}} = 2.5 \text{ m s}^{-1}$. Since no added pipes are part of a loop and the mass flows in the EHs are fixed for each time step k, finding the diameter can be performed for each added pipe separately. For each added pipe $p \in \mathcal{E}_{\mathrm{top}}^{\mathrm{opt}} \setminus \mathcal{E}_{\mathrm{top}}^{\mathrm{sq}}$ and each $d \in D$ the time step with the highest demand is simulated. Each simulation results in a velocity $v_p(d)$. For each pipe the diameter is chosen that results in the lowest deviation from v_{des}.

3.3. Adding additional generating units

In the case a DHN is extended, there might be the need to add additional producers. Furthermore, a different type of producer will alter the fuel cost of the system (e.g., an LSHP compared to a CHP plant). Due to the lack of available space in most metropolitan areas, it is assumed that new producers are always added at the same nodes where producers already exist.

3.4. Operation of generating units

The operation of the producers has a significant influence on the power losses of the DHN and therefore on the fuel cost. Especially the supply temperature $T_{\mathrm{t}}^{\mathrm{PR}}$ and the mass flow $\dot{m}_g$ at each producer g influence the losses of the DHN. The link between DHN heat supply $\dot{Q}_{\mathrm{DHN}}^{g}$ of generator g, $T_{\mathrm{t}}^{\mathrm{PR}}$, $\dot{m}_g$, and the return temperature $T_{\mathrm{o},g}^{\mathrm{PR}}$ at the generator is given by [46]

$$\dot{Q}_{\mathrm{DHN}}^{g}(k) = c_{\mathrm{w}} \dot{m}_g(k) \left(T_{\mathrm{t}}^{\mathrm{PR}}(k) - T_{\mathrm{o},g}^{\mathrm{PR}}(k)\right),$$

resulting from the first law of thermodynamics assuming a constant heat capacity of water $c_{\mathrm{w}} = 4190 \text{ J kg}^{-1} \text{ K}^{-1}$ and a constant density of water $\rho = 997 \text{ kg m}^{-3}$.

The heat production for the DHN at one main producer $g = 1$ is controlled by setting the mass flow

$$\dot{m}_1(k) = \dot{m}_{\mathrm{EH}}(k) - \sum_{j=2}^{\left|\mathcal{N}_{\mathrm{top,PR}}^{\mathrm{opt}}\right|} \dot{m}_j(k)$$

in order to fulfill *Kirchhoff's current law* with the sum of the mass flow of all EHs $\dot{m}_{\mathrm{EH}}(k) = \sum_{z \in \mathcal{Z}} \dot{m}_{\mathrm{EH}}^{z}(k)$.

The supply temperature $T_{\mathrm{t}}^{\mathrm{PR}}$ is part of the optimization by altering the two parameters $\boldsymbol{u}_{\mathrm{PR}}^{\top} = \begin{bmatrix} u_{\mathrm{PR}}^{0} & u_{\mathrm{PR}}^{1} \end{bmatrix}$ with $u_{\mathrm{PR}}^{0} \in \mathbb{R}_{>0}$ and $u_{\mathrm{PR}}^{1} \in \mathbb{R}_{\leq 0}$ influencing the supply temperature

$$T_{\mathrm{t}}^{\mathrm{PR}}(k) = u_{\mathrm{PR}}^{0} + u_{\mathrm{PR}}^{1} \hat{T}_{\mathrm{air}}(k) \tag{4}$$

at time step k, where $\hat{T}_{\mathrm{air}}(k)$ is the average daily outdoor temperature. Hence, $T_{\mathrm{t}}^{\mathrm{PR}}$ is constant during each day. Using a heat characteristic defined by (4) is a common operating procedure for DHNs. See, for example, [47].

The mass flow $\dot{m}^z_{\mathrm{EH}}(k)$ in each EH z is given by

$$\dot{m}^z_{\mathrm{EH}}(k) = \max\left\{ \frac{\dot{Q}^z_{\mathrm{DHN}}(k)}{c_{\mathrm{w}}\left(T^{\mathrm{PR}}_{\mathrm{t}}(k) - T_{\mathrm{r}}\right)}, \dot{m}^{\min}_{\mathrm{EH}} \right\}$$

with the heat demand $\dot{Q}^z_{\mathrm{DHN}}$ of EH z and a fixed return temperature $T_{\mathrm{r}} = 70\ ^\circ\mathrm{C}$. The mass flow $\dot{m}^z_{\mathrm{EH}}$ is bounded from below by $\dot{m}^{\min}_{\mathrm{EH}}$ in order to prevent low flow velocities which otherwise would result in high power losses in relation to the low heating demands.

The mass flow of a producer depends on the producer type. Three different producer types are considered: waste incineration plants, CHPs, and LSHPs. All models are described in Appendix B.3.

3.5. Running the simulation

The simulation of all three networks is performed in *pandapower* [39] and *pandapipes* [44]. All three networks are simulated using a quasi-stationary approach that makes use of common nonlinear equations. This approach calculates all relevant variables, such as voltages, currents, mass flows, pressure values, and temperatures, for each node or branch. The reader is referred to the documentation of the two tools for more details. For the simulation of the DHN and the gas network the friction model by Nikuradse is used, valid for turbulent, fully developed rough flows [48]. Both tools use a Newton-Solver for solving each system of nonlinear algebraic equationsSNAE.

One representative year is simulated. The temperature losses of the DHN depend on the soil temperature. The length of a time-step Δt has a significant influence on the time it takes to simulate all three networks for one year. Hence, a trade-off has to be made between accuracy of the simulation and simulation time. A time step length of $\Delta t = 2$ h is chosen for the simulations, which results in a simulation time of approximately 3 min for simulating one year.

4. Optimization

As [8] pointed out, a simulation within the objective function is more flexible in order to represent the processes of an interconnected energy network. This comes with the drawback that no gradient to a simulation exists. Hence, a gradient-free optimization approach must be used.

4.1. Objective functions

Comparable to the approach in [8] our focus is on two objective functions. The first objective

$$J_{\mathrm{cost}} = \sum_{j\in C_{\mathrm{inv}}} a^{\mathrm{inv}}_j + \sum_{i\in\{\mathrm{el,GAS,O}\}} c^{\mathrm{fuel}}_i + \sum_{i\in\{\mathrm{el,GAS}\}} c^{\mathrm{op}}_i$$

describes the overall cost of the system for one year with the set of invest costs $C_{\mathrm{inv}} = \{\mathrm{HP, DHN, GAS, O, pn, p, LSHP, CHP}\}$. The second objective function

$$J_{CO_2} = \sum_{i\in\{\mathrm{el,GAS,O}\}} c^{CO_2}_i \Delta t \sum_{k=1}^{n_{\mathrm{ts}}} p^{\mathrm{imp}}_i(k)$$

is the CO_2 emission of the interconnected energy system over a time span of one year. Equations for each investment cost are derived in Appendix C.

4.2. Constraints

The number of houses with pellet boilersdecentralized houses in each EH is not part of the optimization variables but is calculated by (1). Hence, the constraint

$$\boldsymbol{y}_{\mathrm{O}} = \boldsymbol{n}_{\mathrm{ho}} - \sum_{t\in\{\mathrm{HP,DHN,GAS}\}} \boldsymbol{y}_t \geq \boldsymbol{0} \tag{5a}$$

has to hold.

In many areas the extension or reinforcement of energy systems is a challenge. In order to represent these challenges additional constraints are added. Based on (C.2), constraining the overall construction of DHN pipes is achieved by

$$\sum_{e\in(\mathcal{E}_{\mathrm{opt}}\setminus\mathcal{E}_{\mathrm{sq}})} l(e) + \sum_{z\in\mathcal{Z}} l^z_{\mathrm{p}}(y^z_{\mathrm{DHN}} - y^z_{\mathrm{DHN,sq}}) = l^{\mathrm{opt}}_{\mathrm{DHN}} \leq n_{\mathrm{py}} r_{\mathrm{p}} \tag{5b}$$

with n_{py} the number of planning years and r_{p} the maximum pipe length added per year. The same thoughts lead to a restriction of the LV and MV electric energy network extension represented by

$$\sum_{p\in\mathcal{L}_v} l^p_{\mathrm{PC}} n^p_{\mathrm{new}} = l^{\mathrm{opt}}_v \leq n_{\mathrm{py}} r_v, \quad v \in \{\mathrm{LV, MV}\} \tag{5c}$$

with r_v the maximum power line length of voltage level v added per year and $\mathcal{L}_v$ the set of power lines in voltage level v. For each heating option $t \in \{\mathrm{HP, GAS, O}\}$ the number of newly built heating systems is constrained by

$$\sum_{z\in\mathcal{Z}} \Delta y^z_t \leq n_{\mathrm{py}} s_t \tag{5d}$$

with $\Delta y^z_t = y^z_t - y^z_{t,\mathrm{sq}}$ and s_t being the maximum number of heating systems of type t that can be connected within one year. For DHN house stations there is no constraint since it is assumed that the pipe extension is the more restrictive constraint.

In addition, it has to be ensured that the simulation of the DHN is physically feasible, i.e., the return temperature T^z_{t} of zone z is not allowed to be lower than minimum temperature $T_{\min} = 30\ ^\circ\mathrm{C}$. Therefore, the constraint

$$\sum_{k=1}^{n_{\mathrm{ts}}} \begin{cases} 1, & \min_{z\in\mathcal{Z}} T^z_{\mathrm{t}}(k) < T_{\min}, \\ 0, & \text{otherwise} \end{cases} \leq 70 \tag{5e}$$

is introduced. In maximum of 70 time steps the lowest return temperature $\min_{z\in\mathcal{Z}} T^z_{\mathrm{t}}(k)$ is allowed to be lower than $T_{\min}$, since *pandapipes* only allows for quasi-stationary simulations. Quasi-stationary simulations neglect the capacitive properties of DHNs, i.e., they result in a less damped system dynamic.

4.3. Optimization algorithm

In this work the results of two optimization algorithms are combined: a surrogate and a genetic algorithm. *ParMOO* is a surrogate optimizer implemented in Python for solving constrained multi-objective optimization problems [49]. Surrogate optimization algorithms are designed for optimization problems with computationally expensive objective functions, e.g., objective functions containing a simulation [25]. The surrogate model is a *Gaussian radial basis function*. The search technique for finding initial samples for fitting the surrogate is *Latin hypercube sampling*. *Generalized pattern search* is used for generating optimal samples within the surrogate, since it does not require a gradient of the objective function.

pymoo is a library for single and multi-objective optimization in Python [50]. The algorithm *NSGA-II* implemented in *pymoo* based on [51] is used in this work with a population size of 1000. NSGA-II is a non-dominated sorting genetic algorithm.

Both algorithms are initialized with the same design parameter combinations in order to reduce simulation time. All simulation results generated by both algorithms are saved. Based on all available simulation results that do not validate any of the constraints (5) a Pareto front is constructed by varying the CO_2 price. For each $c \in \mathcal{O}$ the design parameter combination $\boldsymbol{x}_x$ with the lowest $J(\boldsymbol{x}_x) = J_{\mathrm{cost}}(\boldsymbol{x}_x) + cJ_{CO_2}(\boldsymbol{x}_x)$ is selected. The set of CO_2 prices

$$\mathcal{O} = \{3.99\ €/tx \mid \forall x \in \{0, 1, \ldots, 500\}\}$$

results in a maximum CO_2 price of 1995 €/t which is ten times the predicted CO_2 price for Germany in 2045 [52].

Table 1
Parameters of the zones.

EH	Q in TW h	E in TW h	$\frac{Q_i}{A_i}$ in kW h/m^2	$y_{\mathrm{DHN,sq}}$	$y_{\mathrm{HP,sq}}$	$y_{\mathrm{GAS,sq}}$	$y_{\mathrm{O,sq}}$	$l_{\mathrm{p,EH}} l_p$ in m
A	0.227	0.087	2.466	0	1 800	11 300	5 150	20.2
B	0.730	0.251	7.939	0	2 900	21 400	2 750	18.42
C	3.642	1.174	65.97	12 800	3 050	13 100	2 850	14.82
D	4.075	1.3	110.737	14 950	2 650	8 250	0	6.8
E	0.12	0.046	2.183	0	1 500	4 250	3 100	26.8
F	0.285	0.11	5.17	0	3 750	14 900	6 400	19.12
G	3.198	1.027	57.93	14 750	2 400	10 100	0	15.64
H	0.898	0.298	16.265	0	2 550	14 650	1 600	17.26
I	3.339	1.057	36.29	0	4 350	34 100	4 100	16.46
J	0.307	0.12	2.084	0	3 000	9 750	11 800	24

Table 2
Parameters of the producers of the status quo IES. The junctions are depicted in Fig. 4.

j	junctions			$\dot{Q}^j_{\mathrm{max}}$ in MW	η^j_{el}	η^j_{h}
	DHN	el	gas			
CHP 1	1	1	7	550	0.45	0.47
waste	10	5		420	0.63	0.27
CHP w	10	5	4	420	0.3	0.6
CHP 2	4	3	5	150	0.3	0.6
CHP 3	7	9	1	150	0.3	0.6
CHP 4	2	1	6	150	0.3	0.6
CHP 5	3	1	6	150	0.3	0.6
CHP 6	5	4	4	150	0.3	0.6
CHP 7	8	9	1	150	0.3	0.6

5. Case study

The case study considered in this work has approximately the size of the city of Hamburg, Germany. The area comprises 250 000 houses dissected into $n_{\mathrm{EH}} = 10$ zones. To speed up the optimization, 50 houses are modeled with the same demand profiles and a collective decision is made on the heating technology for these houses. Nevertheless, this procedure is not required in order to use the presented approach. The goal of the planning process is to identify the optimal IEN that can be constructed within a five-year timeframe. The parameters of the zones are displayed in Table 1, and the data of the producers in Table 2. Fig. 4 illustrates the topology of the three overlying networks, as well as the potential additional connections of the DHN.

The set of additional producers $\mathcal{Y}_{\mathrm{opt}}$ consists of a LSHP at DHN junction 1 and electric energy network junction 1 and a CHP at DHN junction 1, electric energy network junction 1, and gas network junction 7. Only the maximum heating power $y_{\mathrm{PR}}^{\mathrm{LSHP}}$ of the LSHP is part of y_{PR}, i.e., $y_{\mathrm{PR}} = y_{\mathrm{PR}}^{\mathrm{LSHP}}$. If the required heating power $\dot{Q}_1$ at DHN junction 1 exceeds $\dot{Q}_{\mathrm{max}}^{\mathrm{CHP1}} + y_{\mathrm{PR}}^{\mathrm{LSHP}}$, a new CHP is built with

$$\dot{Q}_{\mathrm{max}}^{\mathrm{CHP,new}} = 50\ \mathrm{MW} \left\lceil \frac{\dot{Q}_1 - \dot{Q}_{\mathrm{max}}^{\mathrm{CHP1}} + y_{\mathrm{PR}}^{\mathrm{LSHP}}}{50\ \mathrm{MW}} \right\rceil .$$

Therefore, the optimization problem has 33 design variables.

In the following, the results of the multi-objective optimization applied to the case study are discussed. First, a detailed analysis of a number of solutions identified on the Pareto front is performed. Then, conclusions are drawn regarding the heating technologies, the supply temperature parameters, the generation units, and the required power import.

5.1. Pareto front

The Pareto front resulting from solving the constrained multi-objective optimization problem and a selection of respective optimal input variables is illustrated in Fig. 5. The top plot in Fig. 5 shows the Pareto front and the status quo cost (depicted by the black square). The second plot from the top depicts the total number of heating systems $y_t^{\Sigma} = \sum_{z \in \mathcal{Z}} y_t^z$ of type $t \in \{\mathrm{HP}, \mathrm{DHN}, \mathrm{GB}, \mathrm{O}\}$ in the entire metropolitan area. The third and fourth plots from the top show the number of added heating technologies Δy_t^{A} and Δy_t^{C} for each type t in zone A and zone C, respectively. Zones A and C were chosen for a detailed analysis of the optimization results because zone A is a less densely populated area that is not supplied by the DHN but is close to the DHN, and zone C is a densely populated zone that is already supplied by the DHN. The fifth diagram in Fig. 5 shows the optimal operational planning variables $\boldsymbol{u}$ corresponding to each Pareto point. The last diagram shows the required LV line and DHN pipe extensions resulting from each optimal choice of design variables.

Six solutions (**1**–**6**) are more optimal in terms of J_{cost} than the status quo (indicated by the black square). The low annualized costs for solutions **1** ($J_{\mathrm{cost}} = 568.46\ mil.€$) and **2** ($J_{\mathrm{cost}} = 568.59\ mil.€$) can be attributed to an increase in DHN houses in zone C by $\Delta y_{\mathrm{DHN}}^{\mathrm{C}} = 7200$ houses (indicated in the fourth plot from the top in Fig. 5). Due to the increase in DHN houses, the annualized investment costs corresponding to **1** and **2** are higher than the investment costs of the status quo IEN (Fig. 6). Note, that the status quo IEN has investment costs for gas and pellet boilers (indicated by filled markers in Fig. 6), since heating technologies older than a specified age need to be replaced (explained in more detail in Appendix C.1). In solutions **1** and **2**, the investment costs for gas and pellet boilers are lower than in the status quo IEN, because a part of the gas and pellet boilers are replaced by DHN HSs and HPs.

The increase in houses connected to the DHN leads to an increase in CHP production (Fig. 7(a)) compared to the status quo IEN (Fig. 7(b)). As a result, the amount of imported electric energy is reduced. The average electricity price is 44.49 €/MW, which is more than twice the constant gas price of $\hat{c}_{\mathrm{GAS}}^{\mathrm{fuel}} = 19.4\ €/MW$. Thus, the total annualized cost of the system is reduced by increasing the DHN load, which in turn reduces the amount of imported electric power. In contrast, gas imports are increased.

The increase in the number of houses connected to the DHN necessitates the construction of a CHP at junction 1. An LSHP is built next to the CHP. The addition of an LSHP is counterintuitive due to the high average electricity prices. However, the LSHP is only utilized in single time-steps (Fig. 8(a)) with low electricity prices.

With decreasing CO_2 emissions, the number of HPs in the metropolitan area increases, as can be seen in the second plot from the top in Fig. 5. Solution **8** requires the installation of 23 350 additional HPs. For comparison: 27 950 houses of the status quo IEN are supplied by HPs, and the total number of additional HPs within the planning horizon is constrained to 32 000. The share of all other heating technologies is diminished. The number of gas boilers is reduced by 6750, pellet boilers by 16 250, and DHN HSs by 350. Solution **8** requires annualized investment costs of 60.83 mil.€, which is twice the annualized investment cost of the status quo IEN.

The significant difference of 78.829 mil.€between the total cost of solutions **8** and **9** can be attributed to a notable shift in HP installations from less densely populated areas to areas where a majority of houses

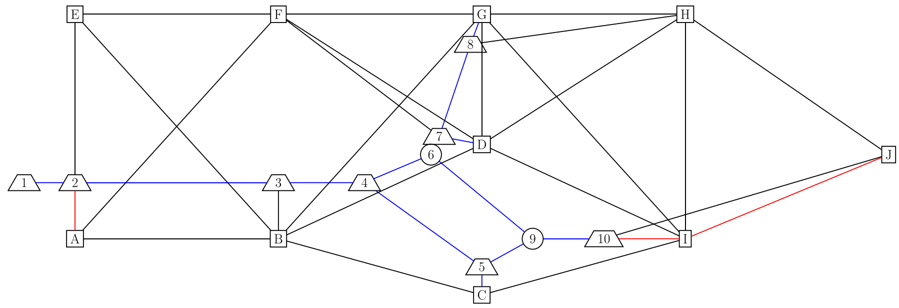

(a) DHN supply line: all nodes and edges drawn represent $\mathcal{G}_{\text{all}}$, $\mathcal{G}_{\text{sq}}$ in blue, if the three EHs represented by the nodes A, I, and J are added to the DHN, $\mathcal{G}_{\text{all}}$ is given by the blue and red edges. Note: some nodes were slightly moved for visibility reasons.

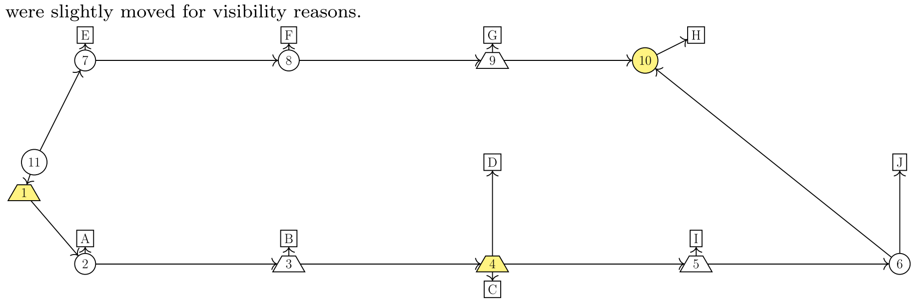

(b) $\mathcal{G}_{\text{el}}$

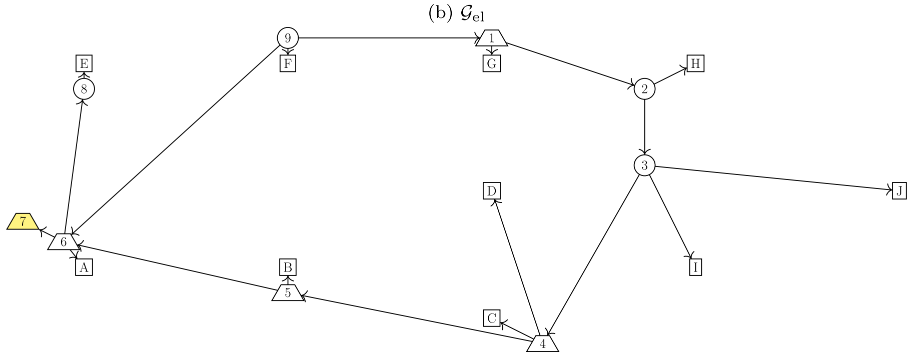

(c) $\mathcal{G}_{\text{GAS}}$

Fig. 4. Energy networks represented by graphs with EH nodes depicted as rectangles and producer nodes as trapezoids. Connection nodes to the higher network level are colored yellow. (For interpretation of the references to colour in this figure legend, the reader is referred to the web version of this article.)

are multi-family homes. This is a consequence of the restriction on the number of additional HP installations. Given the restriction on the number of additional HPs, the optimizer selects the installation of HPs in multi-family houses with a high heating demand. For example, in zone A, 1800 HPs are installed for solution **8**. However, for solution **9**, a solution with a higher cost but lower CO_2 emissions compared with **8**, only 400 HPs are installed in zone A. The opposite is true for zone C. For solution **8**, 2450 HPs are newly added. Solution **9** requires the installation of 23 100 HPs in zone C. The addition of HPs is constrained to a maximum of 32 000, representing 72% of the allowed HPs that are installed in zone C, a densely populated zone with mainly multi-family houses. The annualized investment costs reflect the shift from installing HPs in zones with a high proportion of single-family houses to zones with a high proportion of multi-family houses (Fig. 6). While the total number of newly installed HPs increases from solution **8** to **9** by only 3850 HPs, the annualized cost of all HPs $a_{\text{HP}}^{\text{inv}}$ increases by 58.3%. The addition of 23 100 HPs entails an extension of the LV by 448 km in zone C. The total annualized investment cost for solution **9** is 106.17 mil.€. A comparison of the Sankey diagrams for solution **9** and the status quo IEN (Fig. 7(b) and (c)) reveals that the decrease in CO_2 emissions by 1.241 mil.t (a decrease of 29%) is achieved by lowering the gas import from 18.956 TW h to 12.808 TW h and increasing the imported electric power from 2.717 TW h to 6.774 TW h. This is due to the increase in HPs at the expense of all other heating technologies and due to the reduced relevance of the CHP units.

In order to achieve a reduction in CO_2 emissions of 1.509 mil.t (solution **11** compared with the status quo), the number of pellet boilers is decreased by 4400 in comparison with the status quo IEN (Fig. 5). The pellet boilers are replaced by 2200 HPs and 2200 DHN HSs. Consequently, zone A is added to the DHN. The optimizer determines that zone A should be added, as it is in close proximity to the existing DHN (see Fig. 4(a)). Additionally, zone A is the nearest zone to DHN node 1, which is the node where the LSHP is added.

After analyzing the Pareto front, conclusions are drawn based on the Pareto front regarding the heating technologies, the supply temperature of the DHN, the generation units and the imported power.

5.2. Heating technologies

Pellet boilers. The share of pellet boilers is decreasing across all solutions due to their high costs and significant CO_2 emissions.

DHN house stations. If the focus is solely on cost reduction, increasing the share of DHN heat demand will increase the share of CHP. This shift reduces the need for imported electricity, which in turn reduces the overall cost of the IEN, but at the expense of increased CO_2 emissions (see optimal solutions **1** and **2** in Fig. 5). Solutions **9**, **10**, and **11** reduce

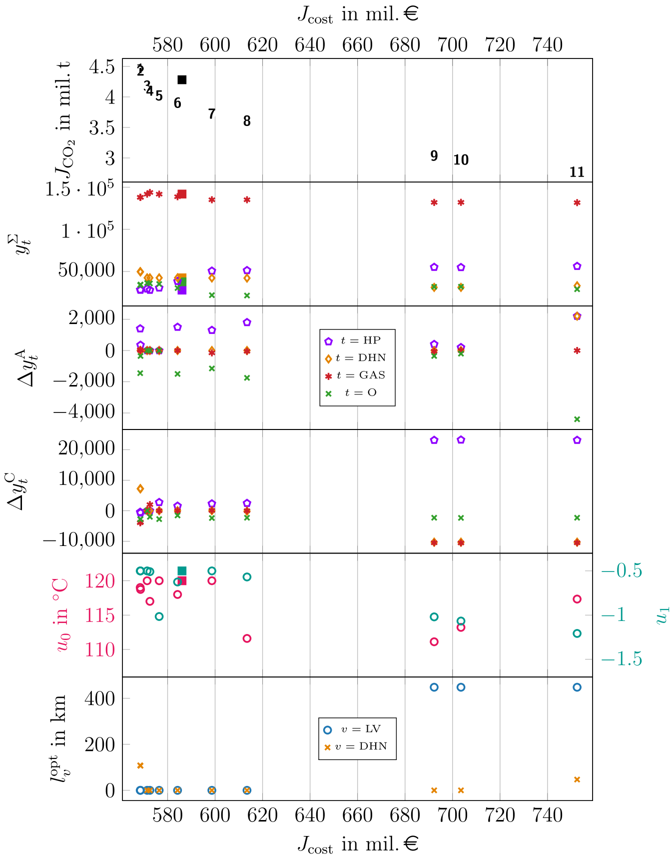

Fig. 5. Pareto front resulting from the co-planning process. Squares represent status quo, black numbers represent the points of the Pareto front. (For interpretation of the references to colour in this figure legend, the reader is referred to the web version of this article.)

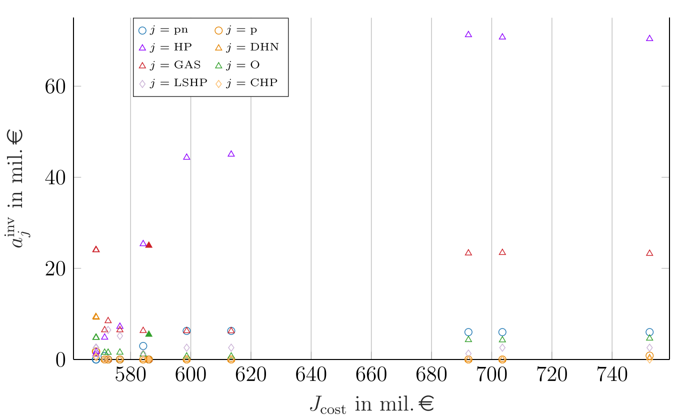

Fig. 6. Annualized investment costs for all simulations that are part of the Pareto front. Transformer and power line investment costs (pn) and pipe investment costs (p) are depicted by circles, heating technologies by triangles and generating units by diamonds. The investment costs of the status quo IEN are denoted by filled markers.

the number of DHN HSs in the densely populated zone C. This is due to limiting the *number* of added HPs, not the *heating power* of the added HPs. Therefore, the optimizer tends to add HPs in multi-family houses with high heating demand, which are supplied by a high proportion of DHN in the status quo IEN. In contrast, the number of DHN houses is increased in the less densely populated zone A. The optimizer selected zone A as the new DHN zone because it is close to the existing DHN and close to the newly installed LSHP.

Heat pumps. HPs are instrumental in reducing CO_2 emissions. Hence, as the focus on CO_2 emissions increases, the number of HPs increases. For Pareto points with $J_{CO_2} > 3.5\ mil.t$ the increase in HPs mainly takes place in less densely populated zones with single-family houses (for example, zone A). Since the number of HPs is constrained in the optimization, for all Pareto points with $J_{CO_2} < 3.5\ mil.t$, the optimizer shifts from installing HPs in single-family houses to installing HPs in areas with mostly multi-family houses (for example, zone C). This is due to the fact that the CO_2 emission reduction per installed HP is higher in multi-family houses. However, HPs are more expensive than gas-powered solutions, both in terms of fuel cost and initial investment. For six of the eleven Pareto points, HPs are the primary investment cost.

Gas boilers. The number of gas boilers tends to decrease as CO_2 emissions are reduced. However, when the sole objective is to minimize costs rather than CO_2 emissions, the reduction in gas boilers occurs at the expense of DHN HSs. An increase in heating demand supplied by the DHN raises the share of CHP plants, consequently reducing the need for imported electric energy.

5.3. Parameters of the supply temperature

If the focus is on minimizing J_{cost} (solutions **1**-**4**), u_0 falls within the range of 117 °C to 120 °C. As the focus shifts towards J_{CO_2}, u_0 decreases to 111.6 °C (**8**) and 111.12 °C (**9**). In solutions **10** and **11**, u_0 is increased while u_1 is decreased, resulting in higher supply temperatures for cold outdoor temperatures and lower supply temperatures for hot outdoor temperatures.

Fig. 9 depicts the return and supply temperatures of solution **9** between node 1 and EH G over the course of a full year. The supply temperature at node 1 (s1) equals the heat characteristic defined by (4). The return temperature at the second consumer of EH G is between 52 °C and 79 °C. This is high since return temperatures in conventional DHNs are usually between 45 °C and 60 °C, as illustrated in [19]. High return temperatures resulting from high supply temperatures or low mass flows are not beneficial to the efficiency of the DHN, especially the LSHP. Total heat losses in the DHN over the full year are 8.6% for solution **9**.

The high return temperatures are primarily the result of the robust and fast simulation approach. Mass flows at generation units and EHs are calculated prior to the simulation based on typical supply and return temperatures. However, a conservative approach was chosen, setting the return temperature at 70 °C. This results in higher supply temperatures at nodes s1–sG1 than those specified by heat characteristic (4).

5.4. LSHP and CHP plant

A LSHP is installed in all solutions, with the exception of solution **3**. An additional CHP plant is only present in solutions **1** and **2** (Fig. 6), due to the connection of new houses to the DHN. Although the usage of the LSHP is low for all solutions (Fig. 7), an LSHP is preferred over a CHP plant due to its flexibility. This is particularly advantageous when electric energy prices are low, as it allows for the reduction of CHP production and the generation of inexpensive heating power for the DHN. The usage of the LSHP is low, as it is only employed when the cost of electricity is comparatively low in relation to that of natural gas. A more detailed explanation of the control of the LSHP can be found in Appendix B.3.4. The CO_2 emissions do not have an influence on the control of LSHP and CHP plants. In order to integrate the CO_2 emissions into the control of LSHP and CHP plants, a CO_2 price is required. However, a CO_2 price for each solution is the result of the multi-objective optimization and is therefore not previously known.

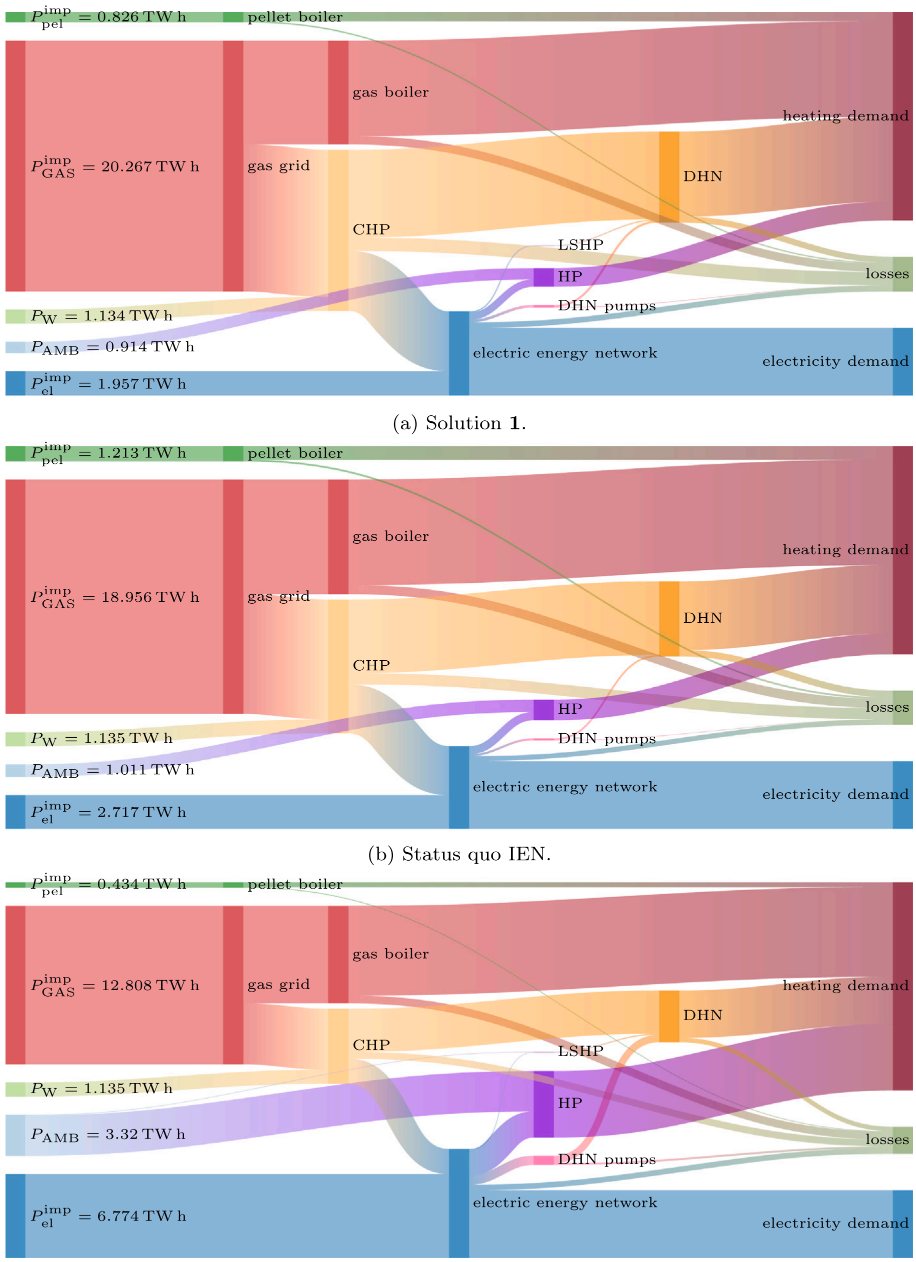

(a) Solution **1**.

(b) Status quo IEN.

(c) Solution **9**.

Fig. 7. Sankey diagrams for status quo IEN and solutions **1** and **9**.

5.5. Imported power

In comparison to the status quo IEN, the annual gas import is increased by 1.311 TW h for solution **1**. In solution **9**, the annual gas import is reduced by 6.148 TW h. As the emphasis on J_{CO_2} relative to J_{cost} increases, the quantity of imported gas per year declines.

As the DHN heating demand determines the electric power generation of the CHP plants, the power import is low during the winter season and high during the summer season for solution **1** (Fig. 8(a)). The annual gas demand of the CHP plants is reduced by 6.951 TW h for solution **9** in comparison to solution **1**. The reduced electric power generation of the CHP plants and the increased electric power demand during the winter season by the HPs result in an almost constant daily electric power import (Fig. 8(b)).

Compared with the status quo, the CO_2 emissions of solution **9** are reduced by 1.15 mil.t. As can be seen in Fig. 7(c), the reduction of the CO_2 emissions is achieved by lowering the amount of imported gas, again achieved by the construction of HPs and the reduction of gas used for the operation of CHP plants. The high share of HPs results in a more efficient system with a reduction of energy losses of 1.013 TW h and an increase of used ambient energy of 2.66 TW h. This is in line with the finding of [53] that efficiency plays a major role in decarbonizing energy systems.

6. Discussion

This section discusses the proposed optimization method and the case study results. The results clearly demonstrate the ability of the proposed

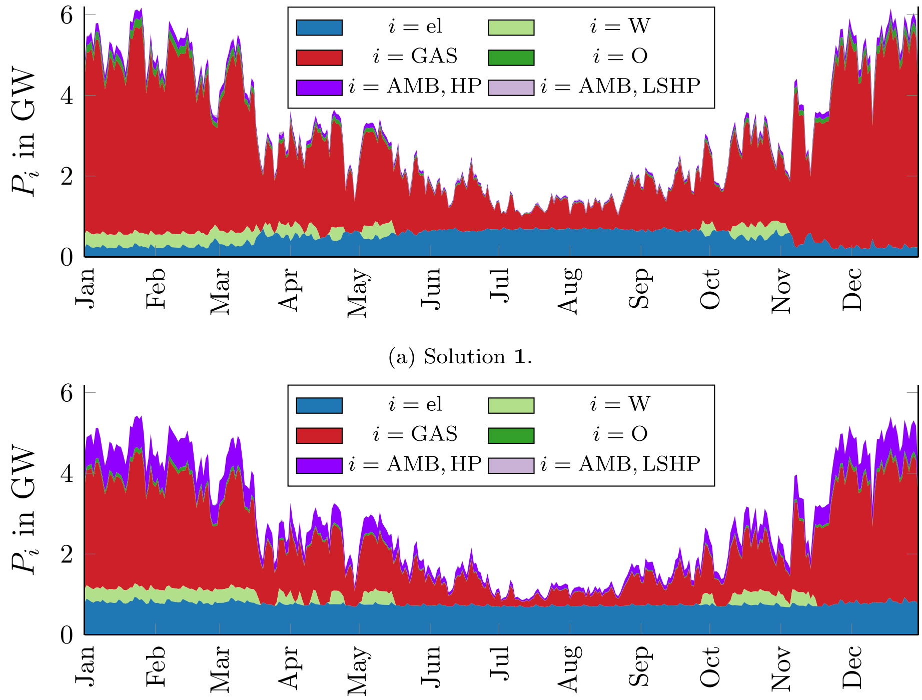

(a) Solution **1**.

(b) Solution **9**.

Fig. 8. Imported power for solutions **1** and **9**. The trajectories represent the mean power values for each day.

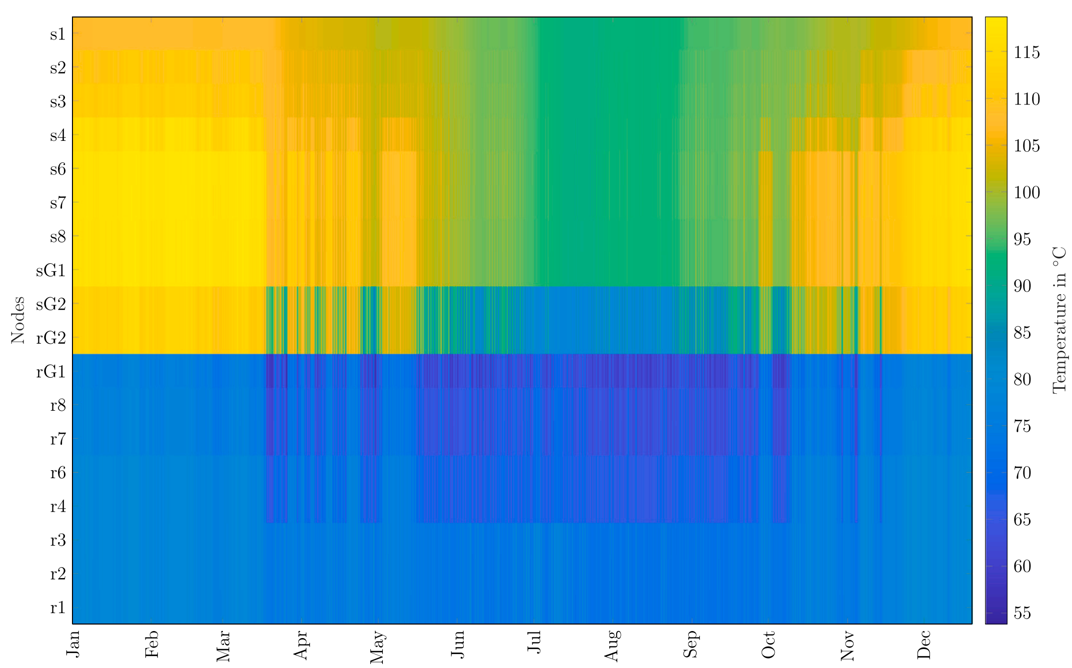

Fig. 9. Node temperatures of DHN supply and return nodes between node 1 and EH G for solution 9. Node names on the *y*-axis are given in the form *s* for supply, *r* for return plus node ID. The node ID is consistent with Fig. 4(a). The node *G* has two supply and return temperatures due to the EH model.

method to plan the decarbonization of a metropolitan area using physical network models. These models allow for the accurate calculation of losses and the limits of existing pipes or power lines. For instance, connecting EH A to the DHN for solutions **10** and **11** demonstrates that proximity to the DHN and to the LSHP within the DHN plays significant roles. Optimization approaches without a physical network model cannot accurately represent these aspects. The results provide interesting insights into the economic and ecological benefits of various heating technologies; however, these results depend heavily on the assumed prices. In our results, high electricity prices favor DHN and not HPs.

However, prices are not the only factor; the parameters of the simulation also impact the results. This is especially true for the number of zones. This is particularly evident when it comes to the number of zones. A limited number of zones results in significantly higher costs for a single zone's LV grid extension. In addition, a constant flow velocity was used to dimension pipes, and a safety margin was added to the return temperatures to calculate the mass flows at the energy hubs (EHs) and generation units. The safety margin results in robust simulations, which is important due to topology changes, as well as high return temperatures. In *pandapipes*, controllers could ensure an equal supply temperature at all generation unit supply nodes and a low return temperature at the EHs. However, this would increase simulation time. A better option for operating the DHN would be a model predictive controller, as presented in [46], for example. However, this would significantly increase simulation time.

Another limitation is that only one node is considered for an LSHP. To truly decarbonize the DHN, more LSHPs or, for example, hydrogen CHPs are needed. However, this would increase the number of optimization variables. In the case of hydrogen CHPs, it would also introduce price uncertainties due to the need for forecasts of hydrogen prices.

Considering the already complex setup of three different networks using physical models, advanced topics such as the meshed operation of power networks or the addition of low-temperature DHNs not connected to the main DHN could not be considered. Furthermore, the addition of HPs was constrained only by number, not feasibility in specific houses, perhaps due to space limitations.

7. Conclusion

This work presents a constrained multi-objective optimization approach for the co-planning of integrated energy networks. Due to the segmentation of the metropolitan area into zones containing an arbitrary number of houses, the approach is scalable. In addition, the approach incorporates the already existing energy networks of the area of interest.

The approach was evaluated through a case study. The case study is a metropolitan area comprising 250 000 houses, which have been divided into ten zones. If the focus is on low investment, operational, and fuel costs, the share of the district heating network increases compared with the status quo. The optimizer selected a densely populated zone for increasing the number of district heating network connections. An increased focus on CO_2 emissions results in the addition of heat pumps. In order to achieve the solution with the lowest possible CO_2 emissions, the optimizer connected a zone with a relatively small housing density to the district heating networkDHN. However, this zone is close to the already existing district heating networkDHN and to a newly constructed large-scale heat pump. Consequently, the presented approach is capable of selecting heating technologies for zones based on their characteristics and spatial location.

In future research, the co-planning approach should be validated with real data. In addition, incorporating a larger number of zones may prove beneficial.

CRediT authorship contribution statement

Jonathan Vieth: Writing – review & editing, Writing – original draft, Software, Methodology, Conceptualization. **Johannes Heise:** Writing – review & editing, Validation, Methodology. **Marwan Mostafa:** Writing – review & editing, Validation, Methodology. **Christian Becker:** Supervision, Funding acquisition. **Arne Speerforck:** Writing – review & editing, Supervision, Methodology, Funding acquisition, Conceptualization.

Declaration of Generative AI and AI-assisted technologies in the writing process

During the preparation of this work, the authors used DeepL Write in order to improve language and readability. After using this tool, the authors reviewed and edited the content as needed and took full responsibility for the content of the published article.

Declaration of competing interest

The authors declare that they have no known competing financial interests or personal relationships that could have appeared to influence the work reported in this paper.

Acknowledgements

This research is supported by the German Federal Ministry of Economic Affairs and Climate Action (BMWK) under the agreement no. 03EWR007O2.

Appendix A. Modeling district heating networks

When modeling the DHN two different approaches are required. The *topological model* only considers the supply line of the DHN. The *simulation model* includes both the supply and the return lines of the DHN. However, both models utilize graphs to represent the DHN.

A.1. Topological model

In contrast to the electric energy and gas network, the topology of the DHN is influenced by the optimizer, since not all EHs are connected to the DHN at the beginning of the planning process. For the DHN extension analysis performed in Section 3.2, modeling the supply line is sufficient. The topology of a DHN is modeled by a connected, undirected graph $\mathcal{G}_{\mathrm{top}} = (\mathcal{N}_{\mathrm{top}}, \mathcal{E}_{\mathrm{top}})$. Comparable to the modeling of electric energy and gas networks, nodes represent the producers and EHs, as well as simple connection points. The set of nodes representing all EHs is given by $\mathcal{N}_{\mathrm{EH}}$ with $|\mathcal{N}_{\mathrm{EH}}| = |\mathcal{Z}|$. The topology of the *status quo* DHN is modeled by the connected, undirected graph $\mathcal{G}^{\mathrm{sq}}_{\mathrm{top}} = (\mathcal{N}^{\mathrm{sq}}_{\mathrm{top}}, \mathcal{E}^{\mathrm{sq}}_{\mathrm{top}})$. The EHs $\mathcal{N}^{\mathrm{sq}}_{\mathrm{EH}}$ with $\mathcal{N}^{\mathrm{sq}}_{\mathrm{top}} \supseteq \mathcal{N}^{\mathrm{sq}}_{\mathrm{EH}} \subset \mathcal{N}_{\mathrm{EH}}$ are connected to $\mathcal{G}^{\mathrm{sq}}_{\mathrm{top}}$. At each call of the simulation model (see Fig. 1) a DHN topology is determined, modeled by the connected, undirected graph $\mathcal{G}^{\mathrm{opt}}_{\mathrm{top}} = (\mathcal{N}^{\mathrm{opt}}_{\mathrm{top}}, \mathcal{E}^{\mathrm{opt}}_{\mathrm{top}})$.

A.2. Simulation model

The simulation of the DHN is performed in *pandapipes* [44]. When running a simulation of the supply and return lines of a DHN in pandapipes, the nodes correspond to connection points. Pipes, producers, and EHs are modeled by edges. The simulation model is given by a connected, directed graph $\mathcal{G}_{\mathrm{sim}}$ modeling the supply and the return lines of the DHN. The graph $\mathcal{G}_{\mathrm{sim}}$ is constructed from $\mathcal{G}_{\mathrm{top}}$ by

$$\mathcal{G}_{\mathrm{sim}} = (\mathcal{N}_{\mathrm{sim}}, \mathcal{E}_{\mathrm{sim}}) = \mathcal{G}_{\mathrm{top}} \cup \mathcal{G}_{\mathrm{r}} \cup \mathcal{G}_{\mathrm{EH}} \cup \mathcal{G}_{\mathrm{PR}},$$

with the supply line $\mathcal{G}_{\mathrm{top}}$ and the return line $\mathcal{G}_{\mathrm{r}} = (\mathcal{N}_{\mathrm{r}}, \mathcal{E}_{\mathrm{r}})$. The graphs $\mathcal{G}_{\mathrm{PR}}$ and $\mathcal{G}_{\mathrm{EH}}$ contain all producers and EHs, respectively. The nodes represent the supply and return nodes, while the edges represent the producers and EHs, respectively. The two graphs $\mathcal{G}_{\mathrm{r}}$ and $\mathcal{G}_{\mathrm{top}}$ are isomorphic, i.e., they have the same topology. For a more precise definition of *isomorphisms* see [40]. For each supply node $s \in \mathcal{N}_{\mathrm{top}}$ there is a matching return node $r \in \mathcal{N}_{\mathrm{r}}$ defined by the homomorphism $\Theta : \mathcal{G}_{\mathrm{top}} \to \mathcal{G}_{\mathrm{r}}$ with

$$\Theta_{\mathcal{N}} : \mathcal{N}_{\mathrm{top}} \to \mathcal{N}_{\mathrm{r}},$$

$$\Theta_{\mathcal{E}} : \mathcal{E}_{\mathrm{top}} \to \mathcal{E}_{\mathrm{r}}.$$

Hence, for each $s \in \mathcal{N}_{\mathrm{top,EH}} = \mathcal{N}_{\mathrm{top}} \cap \mathcal{N}_{\mathrm{EH}}$ modeling an EH in $\mathcal{G}_{\mathrm{top}}$ there exists an $r = \Theta_{\mathcal{N}}(s) \in \mathcal{N}_{\mathrm{r}}$ modeling the connection point of the EH to the return line.

The disconnected, undirected graph $\mathcal{G}_{\mathrm{EH}} = (\mathcal{N}_{\mathrm{sim,EH}}, \mathcal{E}_{\mathrm{sim,EH}})$ with $\mathcal{N}_{\mathrm{sim,EH}} = \mathcal{N}_{\mathrm{top,EH}} \cup \mathcal{N}_{\mathrm{r,EH}}$ and

$$\mathcal{N}_{\mathrm{r,EH}} = \left\{ r \mid \forall s \in \mathcal{N}_{\mathrm{top,EH}} : r = \Theta_{\mathcal{N}}(s) \right\}$$

has the set of edges

$$\mathcal{E}_{\mathrm{sim,EH}} = \left\{ e \mid \forall s \in \mathcal{N}_{\mathrm{top,EH}} : e = \left(s, \Theta_{\mathcal{N}}(s)\right) \right\}.$$

The disconnected, undirected graph $\mathcal{G}_{\mathrm{PR}}$ is obtained using the same approach used for $\mathcal{G}_{\mathrm{EH}}$. In Fig. A.10(a) small example is shown.

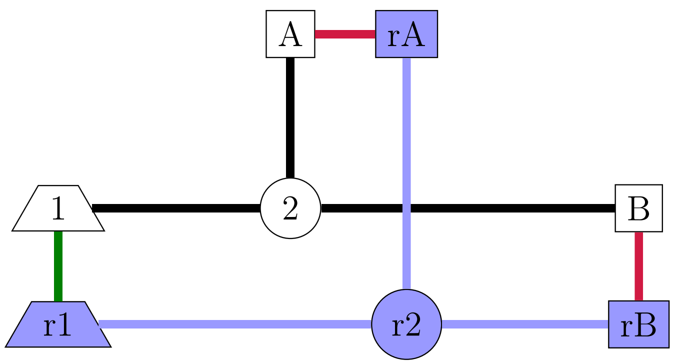

Fig. A.10. Topological and simulation model of a DHN with two EHS and one producer. EH nodes are represented by rectangles, producer nodes by trapezoids, and connection points by circles. $\mathcal{G}_{\mathrm{top}}$ is colored in black, $\mathcal{G}_{\mathrm{r}}$ in blue, $\mathcal{G}_{\mathrm{EH}}$ in red, and $\mathcal{G}_{\mathrm{PR}}$ in green. (For interpretation of the references to colour in this figure legend, the reader is referred to the web version of this article.)

Since $\mathcal{G}_{\mathrm{sim}}$ is a directed graph, for each $e \in \mathcal{E}_{\mathrm{sim}}$ an arbitrary orientation has to be specified.

Appendix B. Simulation details

B.1. Environmental parameters

The temperature data used for the simulation represents the weather in Hamburg in the year 2010. The outdoor temperature is used for calculating the heating demand. The soil temperature is required for calculating the COP of the LSHP and for calculating the heat losses in the DHN. Both temperature profiles are depicted in Fig. B.11.

B.2. Demand profiles

In order to simulate the IEN, heat power loads $P^z_{\mathrm{h},t}(k)$ have to be available for each EH z, each technology $t \in \{\mathrm{HP}, \mathrm{DHN}, \mathrm{GAS}, \mathrm{O}\}$, and each time step k. Optimizing the number of houses connected to a technology instead of finding the optimal heating technology for each house reduces the solution space massively. Hence, a logic is needed for mapping $\boldsymbol{y}_{\mathrm{EH}}$ to the heating technologies of the houses. Since the specific extension cost decreases with the heating demand of a house, the optimizer exchanges the heating technologies of the houses with the highest demand first.

The demand profiles are then given by the weighted sum

$$P^z_t(k) = \sum_{h \in \mathcal{H}^z_t} P^h_{\mathrm{h}}(k) \cdot \begin{cases} \frac{1}{\mathrm{COP}(P^h_{\mathrm{h}}, T_{\mathrm{air}})}, & i = \mathrm{HP}, \\ \eta_t, & \text{otherwise}, \end{cases}$$

with the set of houses $\mathcal{H}^z_t$ in EH z supplied by technology t, the heat load $P^h_{\mathrm{h}}(k)$ of house h, and the efficiency η_t of t. For DHN house stations $\eta_{\mathrm{DHN}} = 1$, for gas boilers $\eta_{\mathrm{GAS}} = 0.92$, and for pellet boilers $\eta_{\mathrm{O}} = 0.92$ is assumed. In the case house h is allocated to the technology HP, $P^h_{\mathrm{h}}(k)$ is divided by the coefficient of performance (COP) [55]

$$\mathrm{COP}(k) = \eta_{\mathrm{C0}} \eta_{\mathrm{PL}} \frac{T_{\mathrm{supply}} + \Delta T}{T_{\mathrm{supply}} - T_{\mathrm{source}}(k) + 2\Delta T}, \tag{B.1}$$

where T_{supply} is the supply temperature of the HP and $T_{\mathrm{source}}(k)$ is the temperature of the heat source of the HP. Assuming an air-water HP is used, $T_{\mathrm{source}}(k)$ corresponds to the ambient outdoor temperature $T_{\mathrm{air}}(k)$ and T_{supply} corresponds to the supply temperature of the supplied building.

As described in [55], η_{C0} and η_{PL} are efficiency factors. The Carnot efficiency factor η_{C0} is assumed to be constant. The part load degradation coefficient η_{PL} is given by

$$\eta_{\mathrm{PL}} = 1 - \psi \left(1 - \frac{P^h_{\mathrm{h}}(k)}{P^h_{\mathrm{h,max}}} \right)$$

with a constant factor $\psi \in (0, 1)$ and the maximum heating power $P^h_{\mathrm{h,max}}$ of the HP in house h [11]. The constant ΔT describes the temperature difference in between T_{supply} and the condenser temperature and T_{source} and the evaporator temperature [55]. It is assumed that $T_{\mathrm{supply}} = 55$ °C, $\eta_{\mathrm{C0}} = 0.6$ [56], $\psi = 0.13$ [57], and $\Delta T = 10$ °C.

B.3. Producer models

B.3.1. Waste incineration model

The model for the waste incineration plants is taken from [58]. The waste incineration plants are used for base generation. However, $\dot{Q}^w_{\mathrm{DHN}}(k)$ of waste incineration plant $w \in \mathcal{Y}_{\mathrm{W}}$ at time step k is flexible in the range $0.7\dot{Q}^w_{\mathrm{max}} \le \dot{Q}^w_{\mathrm{DHN}}(k) \le \dot{Q}^w_{\mathrm{max}}$ with the maximum heat generation $\dot{Q}^w_{\mathrm{max}}$ and the set of waste incineration plants $\mathcal{Y}_{\mathrm{W}}$.

The mass flow in waste incineration plant w is given by

$$\dot{m}_w(k) = \begin{cases} 0, \dot{m}_{\mathrm{EH}}(k) < 0.7\dot{m}^w_{\mathrm{max}}(k) + \dot{m}^1_{\mathrm{min}}, \\ \dot{m}^w_{\mathrm{max}}(k), \dot{m}_{\mathrm{EH}}(k) > \dot{m}^w_{\mathrm{max}}(k) + \dot{m}^1_{\mathrm{min}}, \\ \dot{m}_{\mathrm{EH}}(k) - \dot{m}^1_{\mathrm{min}}, \text{otherwise}, \end{cases}$$

with the minimum mass flow $\dot{m}^1_{\mathrm{min}}$ at the main generator and the maximum mass flow

$$\dot{m}^w_{\mathrm{max}}(k) = \frac{\dot{Q}^w_{\mathrm{max}}}{c_{\mathrm{w}} \left(T^{\mathrm{PR}}_{\mathrm{t}}(k) - T_{\mathrm{r}} \right)}$$

of generator w. The heating power fed into the DHN is calculated by

$$\dot{Q}^w_{\mathrm{DHN}}(k) = c_{\mathrm{w}} \dot{m}_w(k) \left(T^{\mathrm{PR}}_{\mathrm{t}}(k) - T_{\mathrm{r}} \right). \tag{B.2}$$

In accordance with [58], the efficiencies $\eta^w_{\mathrm{el}} = \frac{P^w_{\mathrm{el}}}{P^w_{\mathrm{W}}}$ and $\eta^w_{\mathrm{h}} = \frac{\dot{Q}^w_{\mathrm{DHN}}}{P^w_{\mathrm{W}}}$ are fixed with P^w_{el} being the electric power generation and P^w_{W} the power of the burned waste.

B.3.2. CHP model

The CHP plants considered in this work burn natural gas for the combined heat and power generation. The heat is fully fed to the DHN. The efficiencies $\eta^c_{\mathrm{el}} = \frac{P^c_{\mathrm{el}}}{P^c_{\mathrm{GAS}}}$ and $\eta^c_{\mathrm{h}} = \frac{\dot{Q}^c_{\mathrm{DHN}}}{P^c_{\mathrm{el}}}$ of each CHP plant c are fixed with P^c_{el} representing the electric power generation and P^c_{GAS} the power of the burned gas.

B.3.3. LSHP model

We use the same model for the LSHP as for the HPs in Section B.2. However, $T_{\mathrm{source}}(k)$ in (B.1) is the time dependent soil temperature $T_{\mathrm{soil}}(k)$ and

$$T_{\mathrm{supply},\ell}(k) = \frac{1}{2} \left(T_{\mathrm{t},\ell}(k) + T_{\mathrm{o},\ell}(k) \right)$$

with $T_{\mathrm{t},\ell}(k)$ and $T_{\mathrm{o},\ell}(k)$ being the supply and return temperatures of LSHP ℓ at time step k. In accordance with [5], $\eta_{\mathrm{C0}} = 0.554$ and $\Delta T = 3.742$. Due to a lack of data, part load behavior is neglected, i.e., $\eta_{\mathrm{PL}} = 1$.

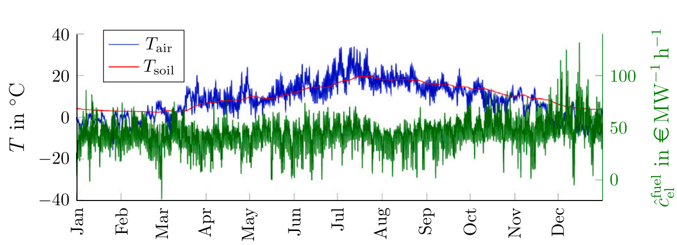

Fig. B.11. Time dependent parameters in the year 2010. Temperature data in red and blue, $\hat{c}^{\mathrm{fuel}}_{\mathrm{el}}$ accessed from [54] (weather data taken from https://www.dwd.de/EN). (For interpretation of the references to colour in this figure legend, the reader is referred to the web version of this article.)

B.3.4. Operation of CHP plants and LSHPs

Since no LSHPs are part of the status quo network and all new producers are built next to existing producers, LSHP ℓ is always built next to CHP c. The combined mass flow $\dot{m}_{\ell c}(k)$ of ℓ and c is calculated by

$$\dot{m}_{\ell c}(k) = \begin{cases} 0, \dot{m}_{\mathrm{EH}}(k) < \dot{m}_{\mathrm{W}}(k) + \dot{m}^{1}_{\mathrm{min}}, \\ \dot{m}_{\mathrm{EH}} - \dot{m}_{\mathrm{W}}(k) - \dot{m}^{1}_{\mathrm{min}}, \text{otherwise}, \end{cases}$$

with $\dot{m}_{\mathrm{W}}(k) = \sum_{w\in\mathcal{Y}_{\mathrm{W}}} \dot{m}_w(k)$ and the heat generation $\dot{Q}^{\ell c}_{\mathrm{DHN}}$ by (B.2). If no LSHP is present next to c, $\dot{Q}^{c}_{\mathrm{DHN}} = \dot{Q}^{\ell c}_{\mathrm{DHN}}$ holds with the heat generation $\dot{Q}^{c}_{\mathrm{DHN}}$ of c. If a LSHP is present a fuel price

$$c^{c}_{\mathrm{CHP}}(k) = \frac{1}{\eta^c_{\mathrm{h}}}\hat{c}^{\mathrm{fuel}}_{\mathrm{GAS}}(k) - \frac{\eta^c_{\mathrm{el}}}{\eta^c_{\mathrm{h}}}\hat{c}^{\mathrm{fuel}}_{\mathrm{el}}(k) \tag{B.3}$$

for c and a fuel price

$$c^{\ell}_{\mathrm{LSHP}}(k) = \frac{\hat{c}^{\mathrm{fuel}}_{\mathrm{el}}(k)}{\mathrm{COP}(k)} \tag{B.4}$$

for ℓ have to be calculated. Based on the fuel prices a decision can be made whether ℓ at time step k is used

$$\dot{Q}^{\ell}_{\mathrm{DHN}}(k) = \begin{cases} 0, c^{c}_{\mathrm{CHP}}(k) < c^{\ell}_{\mathrm{LSHP}}(k), \\ \min\{\dot{Q}^{c}_{\mathrm{DHN}}(k), \dot{Q}^{\ell}_{\mathrm{max}}\}, \text{otherwise}, \end{cases}$$

where $\dot{Q}^{\ell}_{\mathrm{max}}$ is the maximum heating power of ℓ, which leads to $\dot{Q}^{c}_{\mathrm{DHN}}(k) = \dot{Q}^{\ell c}_{\mathrm{DHN}}(k) - \dot{Q}^{\ell}_{\mathrm{DHN}}(k)$. The mass flows are then given by

$$\dot{m}_{\ell}(k) = \frac{\dot{Q}^{\ell}_{\mathrm{DHN}}}{c_{\mathrm{w}}\left(T^{\mathrm{PR}}_{\mathrm{t}}(k) - T_{\mathrm{r}}\right)}$$

and $\dot{m}_c(k) = \dot{m}_{\ell c}(k) - \dot{m}_{\ell}(k)$.

B.4. Parameters of the constraints

Annual expansion limits are required for the constraints presented in Section 4.2. It is assumed that the maximum piping length that can be built per year is $r_{\mathrm{p}} = 40\ km/a$. For the extension of the electric energy network, $r_{\mathrm{LV}} = 160\ km/a$ and $r_{\mathrm{MV}} = 120\ km/a$ are assumed. Furthermore, the limit for newly installed HPs is set to $s_{\mathrm{HP}} = 6400\ /a$ and for pellet and gas boilers to $s_{\mathrm{GAS}} = s_{\mathrm{O}} = 12800\ /a$.

Appendix C. Cost calculation

The goal of the optimization is to minimize fuel cost, operational cost, and capital expenditures (CAPEXs). The annualized CAPEX a^{inv}_j of CAPEX c^{inv}_j is calculated by [59]

$$a^{\mathrm{inv}}_j = \sigma_{\mathrm{debt}} c^{\mathrm{inv}}_j \frac{r}{1-(1+r)^{-\omega_j}} + \sigma_{\mathrm{equity}} \frac{c^{\mathrm{inv}}_j}{\omega_j} \tag{C.1}$$

in order to compare c^{inv}_j with the fuel and the operational costs. The debt and equity ratios are set to $\sigma_{\mathrm{debt}} = 0.29$ and $\sigma_{\mathrm{equity}} = 0.71$ [59] and the interest rate is set to $r = 0.04$ [11]. The lifetime ω_j depends on the nature of investment j and is depicted in Table C.3. In the following, each share of the total cost is derived.

Table C.3
Lifetimes of technologies for calculating annualized costs taken from [4].

technology	ω in years
HP	15
GB	15
O	15
DHN HS	20
pipe	40
transformer	30
power line	30
LSHP	20
CHP	30

C.1. Investment cost

C.1.1. Heating system investment cost

If the optimizer changes the heating system of a house or if the heating system is older than a specified age, costs arise. It is assumed, that a heating system of type $t \in \{\mathrm{HP}, \mathrm{DHN}, \mathrm{GAS}, \mathrm{O}\}$ is replaced, if it is older than $\omega_t + 10\ a$. The cost $c^{\mathrm{inv}}_{t,h}$ for a new heating system depends on the type t and the maximum heating power P^h_{max} of house h, which is equal to the heating demand in the case of $T_{\mathrm{air}} = -8\ ^{\circ}\mathrm{C}$. The cost data for the heating technologies is depicted in Table C.4. For DHN house stations $\hat{c}^{\mathrm{inv}}_{\mathrm{DHN}} = 70\ €/kW$ is assumed.[1] Out of a set $\mathcal{P}_t$ of possible heating system sizes the one with the lowest maximum power $P^h_{\mathrm{max},t}$ which can still provide the power P^h_{max} is chosen, i.e.,

Table C.4
Cost of house heating technologies taken from [60].

(a) Cost of HPs.

$p^{\mathrm{HP}}_{\mathrm{max}}$ in kW	$\hat{c}^{\mathrm{inv}}_{\mathrm{HP}}$ in €/kW
2.4	4229
5.5	1530
8.1	1177
14	906
20	764
30	629
50	548
110	450

(b) Cost of gas boilers. The same cost is assumed for pellet boilers.

$p^{\mathrm{GB}}_{\mathrm{max}}$ in kW	$\hat{c}^{\mathrm{inv}}_{\mathrm{GB}}$ in €/kW
14	570
22	426
30	349
40	289
50	251
60	223
80	185
110	151
160	118

$$P^h_{\mathrm{max},t} = \min\left(\{P \mid \forall P \in \mathcal{P}_t : P \geq P^h_{\mathrm{max}}\}\right).$$

The total cost $c^{\mathrm{inv}}_{t,h}$ of heating technology t for house h is then given by $c^{\mathrm{inv}}_{t,h} = \hat{c}^{\mathrm{inv}}_t(P^h_{\mathrm{max},t})P^h_{\mathrm{max},t}$ with the price per unit power $\hat{c}^{\mathrm{inv}}_t$. Due to the lack of data, for DHN HSs a total cost per house is calculated by $c^{\mathrm{inv}}_{\mathrm{DHN},h} = P^h_{\mathrm{max}}\hat{c}^{\mathrm{inv}}_{\mathrm{DHN}}$. The overall investment cost c^{inv}_t for all new heating systems of type t is given by

$$c^{\mathrm{inv}}_t = \sum_{z\in Z}\sum_{h\in\mathcal{H}^z_t} c^{\mathrm{inv}}_{t,h},$$

where $\mathcal{H}^z_t$ is the set of houses in EH z with a new heating system of type t.

C.1.2. District heating network

We assume, that the pipe cost does not depend on the diameter of each pipe , although this is not necessary for our approach. Possible diameters are $\mathcal{D} = \{0.2\ \mathrm{m}, 0.3\ \mathrm{m}, \ldots, 1\ \mathrm{m}\}$. First, new DHN pipes are built

[1] Cost data provided by local DHN operator.

for connecting the EHs. The total cost of the interconnecting DHN is given by

$$c^{\mathrm{inv}}_{\mathrm{p,inter}} = \hat{c}^{\mathrm{inv}}_{\mathrm{p,inter}} \sum_{e\in(\mathcal{E}_{\mathrm{opt}}\setminus\mathcal{E}_{\mathrm{sq}})} l(e) \tag{C.2a}$$

with the pipe cost $\hat{c}^{\mathrm{inv}}_{\mathrm{p,inter}} = 1500$ €$/m$ per unit length. Second, pipes are built within the EHs for connecting the houses. The length of the added pipes within EH z is not equal to the length of the network representing the DHN within z due to the aggregation (see Section 2.2 for the DHN model within the zones). The sum of the added pipes within the EHs is calculated by

$$c^{\mathrm{inv}}_{\mathrm{p,EH}} = \begin{cases} \hat{c}^{\mathrm{inv}}_{\mathrm{p,EH}} l^z_{\mathrm{p,EH}}(y^z_{\mathrm{DHN}} - y^z_{\mathrm{DHN,sq}}), & y^z_{\mathrm{DHN}} - y^z_{\mathrm{DHN,sq}} > 0, \\ 0, & \text{otherwise} \end{cases} \tag{C.2b}$$

with the linear coefficient $l^z_{\mathrm{p,EH}} \in \mathbb{R}_{>0} l^z_{\mathrm{p}} \in \mathbb{R}_{>0}$ and the pipe cost $\hat{c}^{\mathrm{inv}}_{\mathrm{p,EH}} =$ 500 €$/m$ per unit length [60]. Hence, it is assumed that the DHN piping length increases linearly with the number of newly built DHN house stations. The full cost c_{p} of newly built DHN pipes is then given by $c^{\mathrm{inv}}_{\mathrm{p}} = c^{\mathrm{inv}}_{\mathrm{p,inter}} + c^{\mathrm{inv}}_{\mathrm{p,EH}}$.

C.1.3. Electric energy network

The equipment of buildings with HPs might result in overloads of the transformers and power lines of the electric energy network. Each power line $l \in \{1, 2, \ldots, n_{\mathrm{PC}}\}$ and each transformer $o \in \{1, 2, \ldots, n_{\mathrm{TF}}\}$ has a maximum current i^l_{max} and i^o_{max}, respectively. It is assumed that in regular operation the current in each power line l and in each transformer o is 60% of i^l_{max} and i^o_{max}, respectively. This takes into account the safety margin of the distribution network operators, which is considered, for example, to comply with the N-1 criterion. If the current $i_l(k)$ in power line l at time step k is higher than $0.6 i^l_{\mathrm{max}}$, l has to be reinforced. The same holds for the transformers. The total electric energy network reinforcement cost $c^{\mathrm{inv}}_{\mathrm{pn}}$ is calculated by

$$c^{\mathrm{inv}}_{\mathrm{pn}} = \sum_{l}^{n_{\mathrm{PC}}} \hat{c}^l_{\mathrm{PC}} l^l_{\mathrm{PC}} n^l_{\mathrm{new}} + \sum_{o}^{n_{\mathrm{TF}}} \hat{c}^o_{\mathrm{TF}} n^o_{\mathrm{new}},$$

where $\hat{c}^l_{\mathrm{PC}}$ is the cost per unit length of a power line l, l^l_{PC} is the length of l, $\hat{c}^o_{\mathrm{TF}}$ is the cost of transformer o, and n^a_{new} is the number of new components of the same type as a in parallel to a.

Due to the electric energy network model within the EHs described in Section 2.2.1, n^a_{new} depends on the type of power line or transformer. For example, if a is an overloaded LV-line in EH z, it is assumed that all $m^z_{\mathrm{MV}} m_{\mathrm{LV}} m_{\mathrm{BR}}$ LV-lines in z are overloaded. Hence,

$$n^a_{\mathrm{new}} = \left\lceil \frac{\max\limits_{k\in\{1,2,\ldots,n_{\mathrm{ts}}\}} \left(i_a(k)\right)}{i^a_{\mathrm{max}}} \right\rceil m_a$$

with

$$m_a = \begin{cases} m^z_{\mathrm{MV}} m_{\mathrm{LV}} m_{\mathrm{BR}}, & a \text{ is LV-line in EH } z, \\ m^z_{\mathrm{MV}}, & a \text{ is MV-line in EH } z, \\ 1, & a \text{ is HV-line}, \\ m^i_{\mathrm{MV}} m_{\mathrm{LV}}, & a \text{ is MV/LV-transformer in EH } z, \\ m^z_{\mathrm{MV}}, & a \text{ is HV/MV-transformer in EH } z. \end{cases}$$

The operator $\lceil a \rceil$ rounds a to the next higher integer.

The cost data for the electric energy network expansion is contained in Table C.5.

C.1.4. Additional generating units

LSHPs as well as gas fired CHPs are considered. It is assumed that the cost of both technologies is a linear function of the maximum heating power $\dot{Q}^g_{\mathrm{max}}$, $c^{\mathrm{inv}}_g = \hat{c}^{\mathrm{inv}}_g \dot{Q}^g_{\mathrm{max}}$ with $g \in \{\mathrm{LSHP}, \mathrm{CHP}\}$. For LSHPs a specific cost of $\hat{c}^{\mathrm{inv}}_{\mathrm{LSHP}} = 228000$ €$/MW$ is assumed [60]. According to [4], the specific costs of CHP plants are given by $\hat{c}^{\mathrm{inv}}_{\mathrm{CHP}} = 0.5 \hat{c}^{\mathrm{inv}}_{\mathrm{LSHP}}$.

Table C.5
Electric energy network costs taken from [61].

(a) Cost of power lines.	
powerline type	$\hat{c}_{\mathrm{PC}}$ in €/m
N2XS(FL)2Y 1 × 300 RM/35 64/110 kV	900
NA2XS2Y 1 × 240 RM/25 6/10 kV	120
NAYY 4 × 150 SE	95
(b) Cost of transformers.	
transformer type	$\hat{c}_{\mathrm{TF}}$ in €
63 MVA 110/10 kV	6,300,000
0.63 MVA 10/0.4 kV	44,000

C.2. Operational cost

For the gas network the yearly operational cost $c^{\mathrm{op}}_{\mathrm{GAS}}$ is calculated based on the imported gas power $p^{\mathrm{imp}}_{\mathrm{GAS}}$, i.e., $c^{\mathrm{op}}_{\mathrm{GAS}} = \Delta t \hat{c}^{\mathrm{op}}_{\mathrm{GAS}} \sum_{k=1}^{n_{\mathrm{ts}}} p^{\mathrm{imp}}_{\mathrm{GAS}}(k)$. The operational cost of the electric energy network is assumed to depend on the maximum transformer power, i.e., $c^{\mathrm{op}}_{\mathrm{el}} = \hat{c}^{\mathrm{op}}_{\mathrm{el}} \sum_{o=1}^{n_{\mathrm{TF}}} p^o_{\mathrm{max}}$ with the maximum power p^o_{max} of transformer o. In case of the DHN, the operational cost is calculated based on the pressure difference Δp_u of pump u. One pump is located at each producer and in each EH. The required pumping power is then given by

$$P_{\mathrm{pu}}(k) = \frac{1}{\rho} \left[\sum_{z\in\mathcal{Z}} \dot{m}_z \Delta p_z + \sum_{g\in\mathcal{Y}} \dot{m}_g \Delta p_g \right].$$

Since the pressure losses within the pipes result in an increase in the water temperature [62], $P_{\mathrm{pu}}(k)$ is subtracted from $\dot{Q}^1_{\mathrm{DHN}}$. This is a model inaccuracy, since the temperature increase due to pressure losses occurs throughout the DHN. However, the heat generation within the pipes due to pressure losses is so far not considered in *pandapipes*. The electric power $P_{\mathrm{pu,el}}(k)$ consumed by all pumps is given by $P_{\mathrm{pu,el}}(k) = \frac{P_{\mathrm{pu}}(k)}{\eta_{\mathrm{pu}}}$ with the pump efficiency $\eta_{\mathrm{pu}} = 0.8$ [56].

For the operational cost of the gas network $\hat{c}^{\mathrm{op}}_{\mathrm{GAS}} = 0.078$ €$/MW/h$ and for the operational cost of the transformers $\hat{c}^{\mathrm{op}}_{\mathrm{el}} = 1000$ €$/MW$ is assumed.

C.2.1. Fuel cost

Since all heat consumed in the DHN is generated within the metropolitan area, only electric power, gas, and pellets are imported. The yearly cost for each energy carrier $i \in \{\mathrm{el}, \mathrm{GAS}, \mathrm{O}\}$ is then given by

$$c^{\mathrm{fuel}}_i = \Delta t \sum_{k=1}^{n_{\mathrm{ts}}} \hat{c}^{\mathrm{fuel}}_i(k) p^{\mathrm{imp}}_i(k)$$

with the energy price $\hat{c}_i(k)$ and the imported power $p^{\mathrm{imp}}_i(k)$ of i at time step k.

For the fuel cost a constant pellet price $\hat{c}^{\mathrm{fuel}}_{\mathrm{O}} = 38.7$ €$/MW/h$ [60], a constant gas price $\hat{c}^{\mathrm{fuel}}_{\mathrm{GAS}} = 19.4$ €$/MWh$ [52], and a time-dependent electricity price $\hat{c}^{\mathrm{fuel}}_{\mathrm{el}}$ (Fig. B.11) are assumed. Since the usage of the waste incineration plant depends on the DHN demand, but there is not an infinite amount of waste in the metropolitan area, the combined heat and electric energy production of the waste incineration plant is capped at $E^{\mathrm{max}}_{\mathrm{W}} = 1.135$ TW h. If $E^{\mathrm{max}}_{\mathrm{W}}$ is reached, the gas boiler CHP is used instead.

C.2.2. CO_2 emissions

The CO_2 emissions from the production of all investments are neglected. Hence, only the CO_2 emissions from the imported fuels are considered. The fuel emissions for each energy carrier $i \in \{\mathrm{el}, \mathrm{GAS}, \mathrm{O}\}$ are calculated by

$$c^{CO_2}_i = \hat{c}^{CO_2}_i \Delta t \sum_{k=1}^{n_{\mathrm{ts}}} p^{\mathrm{imp}}_i(k) \tag{C.3}$$

with the CO_2 emission factor $\hat{c}^{CO_2}_i$ of i per unit energy. The data for $\hat{c}^{CO_2}_i$ is taken from [52], i.e., $\hat{c}^{CO_2}_{\mathrm{GAS}} = 0.201 t MW^{-1} h^{-1}$ and $\hat{c}^{CO_2}_{\mathrm{O}} =$

0.165 t MW^{-1} h^{-1}. The CO_2 emission factor for imported electric energy $\hat{c}_{\mathrm{el}}^{CO_2} = 0.0593$ t MW^{-1} h^{-1} is based on the predicted electricity production in Germany in the year 2030 taken from [63] and the CO_2 emission factors taken from [52].

Data availability

The data is publicly available at: https://collaborating.tuhh.de/m21/public/jonathan/gridplanning

References

[1] European Commission, The European Green Deal, Communication from the Commission to the European Parliament, the European Council, the Council, the European Economic and Social Committee and the Committee of the Regions, COM(2019) 640 final, Brussels, 2019.

[2] European Environment Agency, Greenhouse gas emissions from energy use in buildings in Europe, 2023, https://www.eea.europa.eu/en/analysis/indicators/greenhouse-gas-emissions-from-energy?activeAccordion=546a7c35-9188-4d23-94ee-005d97c26f2b (Accessed: 16 May 2024).

[3] Bundesverband der Energie- und Wasserwirtschaft e. V, Wie heizt das Land Hamburg? 2023, https://www.bdew.de/media/documents/BDEW_Heizungsmarkt_2023_Regionalbericht_Hamburg_20250410_W1ygO9C.pdf (Accessed: 16 July 2026).

[4] H. Lund, B. Möller, B.V. Mathiesen, A. Dyrelund, The role of district heating in future renewable energy systems, Energy 35 (2010) 1381–1390, https://doi.org/10.1016/j.energy.2009.11.023

[5] M. Jesper, F. Schlosser, F. Pag, T.G. Walmsley, B. Schmitt, K. Vajen, Large-scale heat pumps: Uptake and performance modelling of market-available devices, Renew. Sustain. Energy Rev. 137 (2021) 110646, https://doi.org/10.1016/j.rser.2020.110646

[6] C.B. Heendeniya, A. Sumper, U. Eicker, The multi-energy system co-planning of nearly zero-energy districts – Status-quo and future research potential, Appl. Energy 267 (2020) 114953, https://doi.org/10.1016/j.apenergy.2020.114953

[7] B. Morvaj, R. Evins, J. Carmeliet, Optimising urban energy systems: Simultaneous system sizing, operation and district heating network layout, Energy 116 (2016) 619–636, https://doi.org/10.1016/j.energy.2016.09.139

[8] T. Falke, S. Krengel, A.-K. Meinerzhagen, A. Schnettler, Multi-objective optimization and simulation model for the design of distributed energy systems, Appl. Energy 184 (2016) 1508–1516, https://doi.org/10.1016/j.apenergy.2016.03.044

[9] J. Vieth, J. Westphal, A. Speerforck, District heating network topology optimization and optimal co-planning using dynamic simulations, Adv. Appl. Energy 19 (2025) 100233, https://doi.org/10.1016/j.adapen.2025.100233

[10] J. Westphal, J. Brunnemann, A. Speerforck, Enabling the dynamic simulation of an unaggregated, meshed district heating network with several thousand substations, Energy 322 (2025) 135434, https://doi.org/10.1016/j.energy.2025.135434, https://www.sciencedirect.com/science/article/pii/S036054422501076X.

[11] D. Hering, A. Xhonneux, D. Müller, Design optimization of a heating network with multiple heat pumps using mixed integer quadratically constrained programming, Energy 226 (2021) 120384, https://doi.org/10.1016/j.energy.2021.120384

[12] R. Bavière, M. Vallée, Optimal Temperature Control of Large Scale District Heating Networks, Energy Procedia 149 (2018) 69–78, https://doi.org/10.1016/j.egypro.2018.08.170

[13] E. Guelpa, V. Verda, Compact physical model for simulation of thermal networks, Energy 175 (2019) 998–1008, https://doi.org/10.1016/j.energy.2019.03.064

[14] D. Shi, D.J. Tylavsky, A Novel Bus-Aggregation-Based Structure-Preserving Power System Equivalent, IEEE Trans. Power Syst. 30 (2015) 1977–1986, https://doi.org/10.1109/TPWRS.2014.2359447

[15] X. Zhang, M. Shahidehpour, A. Alabdulwahab, A. Abusorrah, Optimal Expansion Planning of Energy Hub With Multiple Energy Infrastructures, IEEE Trans. Smart Grid 6 (2015) 2302–2311, https://doi.org/10.1109/TSG.2015.2390640

[16] M. Geidl, G. Koeppel, P. Favre-Perrod, B. Klockl, G. Andersson, K. Frohlich, Energy hubs for the future, IEEE Power Energy Mag. 5 (2007) 24–30, https://doi.org/10.1109/MPAE.2007.264850

[17] E. Guelpa, G. Mutani, V. Todeschi, V. Verda, A feasibility study on the potential expansion of the district heating network of Turin, Energy Procedia 122 (2017) 847–852, https://doi.org/10.1016/j.egypro.2017.07.446

[18] Y. Cao, W. Wei, J. Wang, S. Mei, M. Shafie-Khah, J.P.S. Catalao, Capacity Planning of Energy Hub in Multi-Carrier Energy Networks: A Data-Driven Robust Stochastic Programming Approach, IEEE Trans. Sustain. Energy 11 (2020) 3–14, https://doi.org/10.1109/TSTE.2018.2878230

[19] J. Gustafsson, J. Delsing, J. van Deventer, Improved district heating substation efficiency with a new control strategy, Appl. Energy 87 (2010) 1996–2004, https://doi.org/10.1016/j.apenergy.2009.12.015

[20] C. Hauk, A. Ulbig, A. Moser, Integrated planning of grids and energy conversion units in municipal multi-energy carrier systems, Energy Inform. 4 (2021), https://doi.org/10.1186/s42162-021-00178-0

[21] S. Mashayekh, M. Stadler, G. Cardoso, M. Heleno, A mixed integer linear programming approach for optimal DER portfolio, sizing, and placement in multi-energy microgrids, Appl. Energy 187 (2017) 154–168, https://doi.org/10.1016/j.apenergy.2016.11.020

[22] B. Talebi, P.A. Mirzaei, A. Bastani, F. Haghighat, A Review of District Heating Systems: Modeling and Optimization, Front. Built Environ. 2 (2016) 22, https://doi.org/10.3389/fbuil.2016.00022

[23] C.L.T. Borges, V.F. Martins, Multistage expansion planning for active distribution networks under demand and Distributed Generation uncertainties, Int. J. Electr. Power Energy Syst. 36 (2012) 107–116, https://doi.org/10.1016/j.ijepes.2011.10.031

[24] H. Lu, K. Alanne, I. Martinac, Energy quality management for building clusters and districts (BCDs) through multi-objective optimization, Energy Convers. Manag. 79 (2014) 525–533, https://doi.org/10.1016/j.enconman.2013.12.051

[25] N.V. Queipo, R.T. Haftka, W. Shyy, T. Goel, R. Vaidyanathan, P. Kevin Tucker, Surrogate-based analysis and optimization, Prog. Aerosp. Sci. 41 (2005) 1–28, https://doi.org/10.1016/j.paerosci.2005.02.001

[26] S.H. Żak (Ed), Systems and control, The Oxford series in electrical and computer engineering, Oxford University Press, New York, 2003.

[27] K. Mehlhorn, A faster approximation algorithm for the Steiner problem in graphs, Inf. Process. Lett. 27 (1988) 125–128, https://doi.org/10.1016/0020-0190(88)90066-X

[28] M. Blommaert, Y. Wack, M. Baelmans, An adjoint optimization approach for the topological design of large-scale district heating networks based on nonlinear models, Appl. Energy 280 (2020) 116025, https://doi.org/10.1016/j.apenergy.2020.116025

[29] S. Hossbach, M. Lemke, J. Reiss, Finite-difference-based simulation and adjoint optimization of gas networks, Math. Methods Appl. Sci. 45 (2022) 4035–4055, https://doi.org/10.1002/mma.8030, _eprint: https://onlinelibrary.wiley.com/doi/pdf/10.1002/mma.8030.

[30] Y. Wack, M. Baelmans, R. Salenbien, M. Blommaert, Economic topology optimization of District Heating Networks using a pipe penalization approach, Energy 264 (2023) 126161, https://doi.org/10.1016/j.energy.2022.126161, Num Pages: 10.

[31] J. Vieth, A. Eichler, A. Speerforck, Model Predictive Control of Thermo-Hydraulic Systems Using Primal Decomposition, accepted for publicatio at the IFAC world congress 2026 arXiv:2601.10189, 2026.

[32] Y. Wack, S. Serra, M. Baelmans, J.-M. Reneaume, M. Blommaert, Nonlinear topology optimization of District Heating Networks: A benchmark of a mixed-integer and a density-based approach, Energy 278 (2023) 127977, https://doi.org/10.1016/j.energy.2023.127977, https://www.sciencedirect.com/science/article/pii/S0360544223013713.

[33] L.H. Macedo, J.M. Home-Ortiz, R. Vargas, J.R.S. Mantovani, R. Romero, J.P.S. Catalão, Short-circuit constrained distribution network reconfiguration considering closed-loop operation, Sustain. Energy Grids Netw. 32 (2022) 100937, https://doi.org/10.1016/j.segan.2022.100937, https://www.sciencedirect.com/science/article/pii/S2352467722001825.

[34] J. Heise, M. Engel, M. Mostafa, J. Vieth, D. Babazadeh, A. Speerforck, C. Becker, Coupled Multi-Energy Grid Planning - Paving the Way from Isolated to Integrated Planning, in: 2023 IEEE Belgrade PowerTech, 2023, pp. 1–6, https://doi.org/10.1109/PowerTech55446.2023.10202775

[35] A. Loewen, Entwicklung eines Verfahrens zur Aggregation komplexer Fernwärmenetze: Zugl.: Dortmund, Univ, Diss, 2001, UMSICHT-Schriftenreihe, vol. 29, Fraunhofer-IRB-Verl., Stuttgart, 2001.

[36] F. Strehle, J. Vieth, M. Pfeifer, S. Hohmann, Passivity-Based Stability Analysis of Hydraulic Equilibria in 4th Generation District Heating Networks, IFAC-Pap. 54 (2021) 261–266, https://doi.org/10.1016/j.ifacol.2021.11.088

[37] C. Bordin, A. Gordini, D. Vigo, An optimization approach for district heating strategic network design, Eur. J. Oper. Res. 252 (2016) 296–307, https://doi.org/10.1016/j.ejor.2015.12.049

[38] C. Bode, Simulation of Integrated Energy Systems with a Focus on Gas Grids and Heating Technologies, 2022, https://doi.org/10.15480/882.4192

[39] L. Thurner, A. Scheidler, F. Schafer, J.-H. Menke, J. Dollichon, F. Meier, S. Meinecke, M. Braun, Pandapower—An Open-Source Python Tool for Convenient Modeling, Analysis, and Optimization of Electric Power Systems, IEEE Trans. Power Syst. 33 (2018) 6510–6521, https://doi.org/10.1109/TPWRS.2018.2829021

[40] U. Knauer, K. Knauer (Eds ed), Algebraic graph theory: Morphisms, monoids and matrices, De Gruyter studies in mathematics, second ed, vol. volume 41, De Gruyter, Berlin and Boston, 2019.

[41] A.J. Osiadacz, Simulation and analysis of gas networks, Spon, London, 1987.

[42] R.D. Zimmerman, C.E. Murillo-Sanchez, R.J. Thomas, MATPOWER: Steady-State Operations, Planning, and Analysis Tools for Power Systems Research and Education, IEEE Trans. Power Syst. 26 (2011) 12–19, https://doi.org/10.1109/TPWRS.2010.2051168

[43] X. Liu, J. Wu, N. Jenkins, A. Bagdanavicius, Combined analysis of electricity and heat networks, Appl. Energy 162 (2016) 1238–1250, https://doi.org/10.1016/j.apenergy.2015.01.102

[44] D. Lohmeier, D. Cronbach, S.R. Drauz, M. Braun, T.M. Kneiske, Pandapipes: An Open-Source Piping Grid Calculation Package for Multi-Energy Grid Simulations, Sustainability 12 (2020) 9899, https://doi.org/10.3390/su12239899

[45] A.A. Hagberg, D.A. Schult, P.J. Swart, Exploring Network Structure, Dynamics, and Function using NetworkX, in: Gaël Varoquaux, Travis Vaught, Jarrod Millman (Eds.), Proceedings of the 7th Python in Science Conference, Pasadena, CA USA, 2008, pp. 11–15.

[46] J. Maurer, N. Tschuch, S. Krebs, K. Bhattacharya, C. Cañizares, S. Hohmann, Toward transactive control of coupled electric power and district heating networks, Appl. Energy 332 (2023) 120460, https://doi.org/10.1016/j.apenergy.2022.120460

[47] S. Frederiksen, S. Werner, District Heating and Cooling, Studentlitteratur, 2013.

[48] F.M. White ed. ed., Fluid mechanics, McGraw-Hill Series in Mechanical Engineering, 7. ed, McGraw-Hill, New York, 2011.

[49] T.H. Chang, S.M. Wild, ParMOO: A Python library for parallel multiobjective simulation optimization, J. Open Source Softw. 8 (2023) 4468, https://doi.org/10.21105/joss.04468

[50] J. Blank, K. Deb, pymoo: Multi-Objective Optimization in Python, IEEE Access 8 (2020) 89497–89509.

[51] K. Deb, A. Pratap, S. Agarwal, T. Meyarivan, A fast and elitist multiobjective genetic algorithm: NSGA-II, IEEE Trans. Evol. Comput. 6 (2002) 182–197, https://doi.org/10.1109/4235.996017
[52] 50Hertz Transmission GmbH, Amprion GmbH, TenneT TSO GmbH, TransnetBW GmbH, Netzentwicklungsplan Strom 2037 mit Ausblick 2045: Erster Entwurf der Übertragungsnetzbetreiber, 2023, https://www.netzentwicklungsplan.de/archiv/netzentwicklungsplan-20372045-2023 (Accessed: 16 July 2026).
[53] N. Gerhardt, F. Sandau, S. Becker, A. Scholz, P. Schumacher, D. Schmidt, Heat Transition 2030: key technologies for reaching the intermediate and long-term climate targets in the building sector, 2017, https://www.agora-energiewende.org/publications/heat-transition-2030 (Accessed: 16 July 2026).
[54] Energy-Charts, Electricity production and spot prices in Germany in 2010, 2023,. https://energy-charts.info/charts/price_spot_market/chart.htm?l=en&c=DE (Accessed: 13 June 2023).
[55] A. Speerforck, J. Ling, V. Aute, R. Radermacher, G. Schmitz, Modeling and simulation of a desiccant assisted solar and geothermal air conditioning system, Energy 141 (2017) 2321–2336, https://doi.org/10.1016/j.energy.2017.11.151
[56] D. Hering, M.E. Cansev, E. Tamassia, A. Xhonneux, D. Müller, Temperature control of a low-temperature district heating network with Model Predictive Control and Mixed-Integer Quadratically Constrained Programming, Energy 224 (2021) 120140, https://doi.org/10.1016/j.energy.2021.120140
[57] D.A. Waddicor, E. Fuentes, M. Azar, J. Salom, Partial load efficiency degradation of a water-to-water heat pump under fixed set-point control, Appl. Therm. Eng. 106 (2016) 275–285, https://doi.org/10.1016/j.applthermaleng.2016.05.193
[58] J. Beiron, R.M. Montañés, F. Normann, F. Johnsson, Combined heat and power operational modes for increased product flexibility in a waste incineration plant, Energy 202 (2020) 117696, https://doi.org/10.1016/j.energy.2020.117696
[59] S. Oliva H., M. Garcia G., Investigating the impact of variable energy prices and renewable generation on the annualized cost of hydrogen, Int. J. Hydrog. Energy 48 (2023) 13756–13766, https://doi.org/10.1016/j.ijhydene.2022.12.304
[60] Ministry of the Environment, Climate Protection and the Energy Sector Baden-Württemberg, Kommunale Wärmeplanung: Einführung in den Technikkatalog, 2023, https://um.baden-wuerttemberg.de/fileadmin/redaktion/m-um/intern/Dateien/Dokumente/2_Presse_und_Service/Publikationen/Energie/Kommunale-Waermeplanung-Einfuehrung-in-den-Technikkatalog.pdf (Accessed: 16 July 2026).
[61] Energynautics GmbH, Öko-Institut e.V, Bird & Bird LLP, Verteilnetzstudie Rheinland-Pfalz, 2014, https://mlwuf.rlp.de/fileadmin/14/Themen/Energie_und_Klimaschutz/4._Energieinfrastruktur/Stromnetzausbau/Verteilnetzstudie_RLP.pdf (Accessed: 16 July 2026).
[62] B. van der Heijde, A. Aertgeerts, L. Helsen, Modelling steady-state thermal behaviour of double thermal network pipes, Int. J. Therm. Sci. 117 (2017) 316–327, https://doi.org/10.1016/j.ijthermalsci.2017.03.026
[63] Fraunhofer Institute for Solar Energy Systems, Wege zu einem klimaneutralen Energiesystem, 2021, https://www.ise.fraunhofer.de/de/veroeffentlichungen/studien/wege-zu-einem-klimaneutralen-energiesystem-version-2020-21.html (Accessed: 16 July 2026).